

Competition of deltaic feeder systems reflected by slope progradation: a high-resolution example from the Late Miocene-Pliocene, Drava Basin, Croatia

Špelić, Marko; Kovács, Ádám; Saftić, Bruno; Sztanó, Orsolya

Source / Izvornik: **International Journal of Earth Sciences**, 2023, 112, 1023 - 1041

Journal article, Published version

Rad u časopisu, Objavljena verzija rada (izdavačev PDF)

<https://doi.org/10.1007/s00531-023-02290-w>

Permanent link / Trajna poveznica: <https://um.nsk.hr/um:nbn:hr:169:924634>

Rights / Prava: [Attribution 4.0 International](#) / [Imenovanje 4.0 međunarodna](#)

Download date / Datum preuzimanja: **2025-03-14**



Repository / Repozitorij:

[Faculty of Mining, Geology and Petroleum Engineering Repository, University of Zagreb](#)





Competition of deltaic feeder systems reflected by slope progradation: a high-resolution example from the Late Miocene-Pliocene, Drava Basin, Croatia

Marko Špelić¹ · Ádám Kovács² · Bruno Saftić³ · Orsolya Sztanó²

Received: 13 September 2022 / Accepted: 5 January 2023 / Published online: 24 January 2023
© The Author(s) 2023

Abstract

The thick Lake Pannon sedimentary record provides insights into the downdip and lateral development of stratigraphic surfaces through the analysis of the basin-scale clinoform progradation. The clinoform architecture from the eastern part of the Drava Basin (Pannonian Basin System) was interpreted to reflect the base-level changes. A major downlap surface interpreted as a flooding event followed by rejuvenation of slope progradation was recognized on 2D seismic sections. Detailed 3D seismic interpretation combined with well data revealed that the large sigmoidal and the overlying small oblique clinoform sets that downlap the large one only apparently produce the geometry of a maximum flooding surface. Instead, the 3D mapping revealed the influence of two competing slope systems arriving from the north and northwest. Lateral switching of sediment input, similar to many recent deltaic systems, e.g., Danube and Po rivers led to the variability of stratigraphic surfaces, lithology, and thickness, which resulted in non-uniform shelf-edge migration. These observations were supported by forward stratigraphic modeling simulating different scenarios, which led to the generation of the depositional architecture with an apparent maximum flooding surface. This study also implies the potential pitfalls in basin analysis based only on scarce 2D seismic and emphasizes the role of lateral variations in sediment input controlling the depositional architecture.

Keywords 3D sedimentary architecture · Clinoforms · Stratigraphic surfaces · Forward stratigraphic modeling · Pannonian Basin System

Introduction

The building blocks and sedimentary archives of Earth's past and present basin margins are clinofolds, and their bounding surfaces termed clinoforms (Rich 1951). The high-resolution variability in clinoform geometry reveals the sedimentary processes and the base-level changes along the shelf, slope, and deep-water area (Posamentier and Allen 1999; Helland-Hansen and Hampson 2009; Sztanó et al. 2013a; Jones et al.

2015; Pellegrini et al. 2018; Magyar et al. 2019; Tesch et al. 2019; Paumard et al. 2020; Zecchin and Catuneanu 2020). The factors controlling sedimentary dynamics and architecture were extensively studied in marine settings, which led to the recognition of primary stratal geometries of system tracts and sequences. Several recent studies addressed the effect of along-strike variability in sedimentary systems and its control on system tracts and sequence development (e.g., Helland-Hansen and Hampson 2009; Catuneanu and Zecchin 2016; Madof et al. 2016; Tesch et al. 2019; Zecchin and Catuneanu 2020). The effect was also well addressed in studies dealing with stratigraphical numerical modeling of sedimentary systems and its application in sequence stratigraphy in marine (e.g., Burgess and Prince 2015; Graham et al. 2015; Paumard et al. 2019) and enclosed lacustrine settings (Kovács et al. 2021). Thus, the lateral variability of sediment input represents a significant challenge in basin evolution studies, as it results in contrasting depositional architectures between parallel sections (Posamentier and Allen 1993; Madof et al. 2016). These differences in coeval

✉ Bruno Saftić
bruno.saftic@rgn.unizg.hr

¹ Department of Geology, Croatian Geological Survey, Sachsova 2, 10000 Zagreb, Croatia

² Department of Geology, Institute of Geography and Earth Sciences, Eötvös Loránd University, Pázmány Péter sétány. 1/C, 1117 Budapest, Hungary

³ Department of Geology and Geological Engineering, Faculty of Mining, Geology and Petroleum Engineering, University of Zagreb, Pierottijeva 6, 10000 Zagreb, Croatia

successions are easily visualized by seismic-scale clinoforms (Kovács et al. 2021).

The Late Neogene Lake Pannon sedimentary record in the Pannonian Basin System (PBS) is suitable for studying the details of clinoform progradation (e.g., Vakarcs et al. 1994; Sacchi et al. 1999; Uhrin and Sztanó 2012; Magyar et al. 2013, 2019; Sztanó et al. 2013a). Several coeval sediment feeder systems filled the deep Lake Pannon, gradually accreting a large sedimentary prism, thus building a wide depositional shelf, and generated several hundred-meter-high shelf slopes prograding from 10 to 4 Ma over 600 km (Fig. 1a and b). In addition to the location of sediment feeder systems, the direction of slope progradation was driven by the deepest basin centers (cf. Törő et al. 2012). It is easy to find locations where the

slopes prograding in different directions interacted, which may have influenced the depositional architecture (Fig. 1b; Magyar and Sztanó 2008). One such location could be the Drava Basin in the SW part of the PBS, where the Paleo-Danube (PDu) shelf-slope prograded from the north and united with the Paleo-Drava (PDr) shelf-slope from the NW (Fig. 1b).

To study the youngest Late Miocene to Pliocene clinoforms in this part of Lake Pannon, 3D seismic reflection and well data were used, available due to extensive oil and gas exploration in the Drava Basin. Reinterpreting the vintage well data with the new (3D) seismic allows the identification of the co-existence and the related large-scale architecture of the two confluent, obtuse-angle slope systems. It also

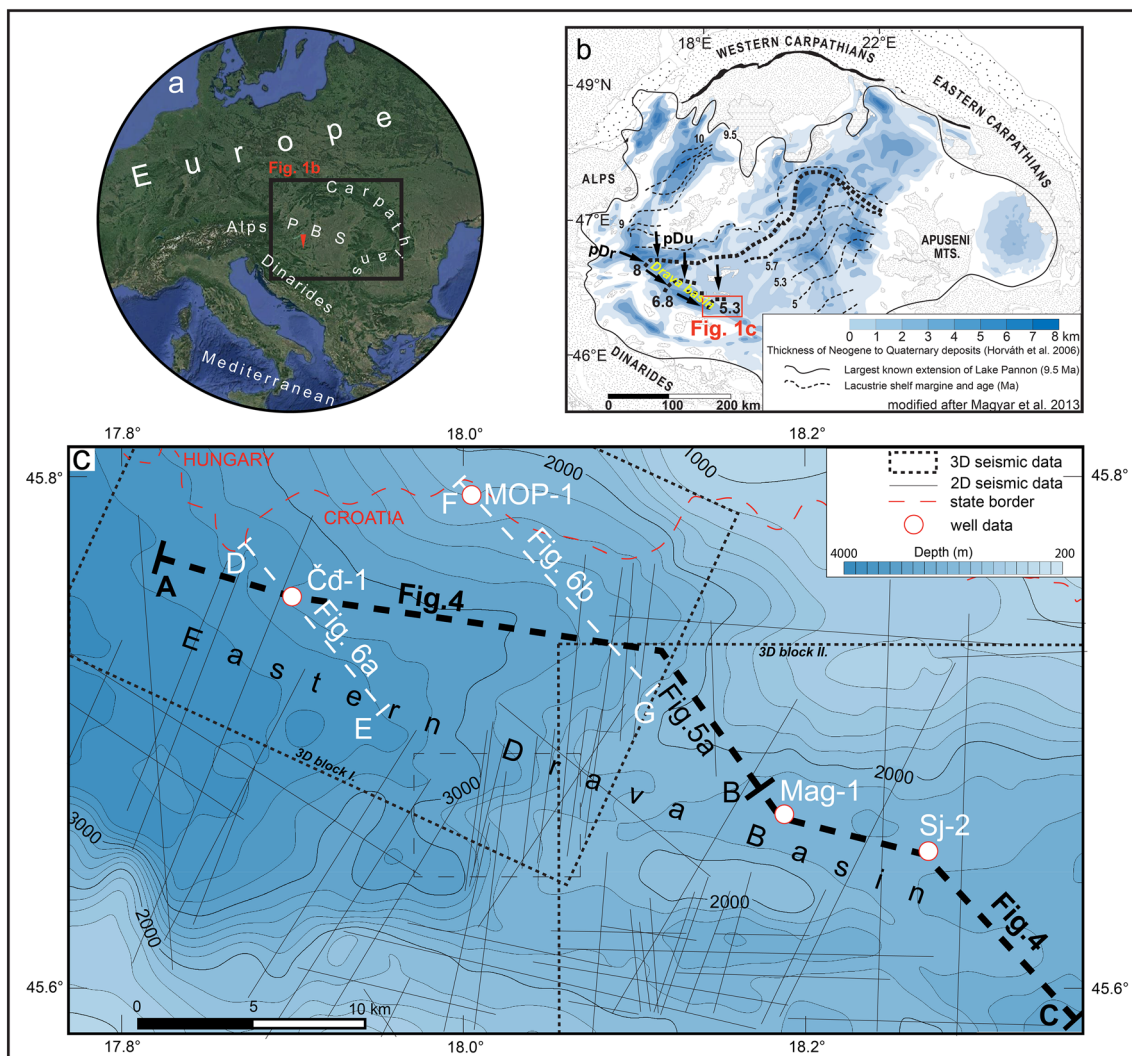


Fig. 1 **a** Location of the Pannonian Basin System and the surrounding orogens. **b** The extent of Lake Pannon and its progradational shelf migration overlain on the thickness map of the Neogene to Quaternary basin-fill. **c** The depth of the basal surface of the lacus-

trine basin-fill succession in the eastern part of the Drava Basin with reflection seismic grid and well data used (<https://www.google.com/intl/hr/earth/>)

facilitated numerical modeling to check different controls on the depositional architecture.

Seismostratigraphic interpretation revealed the existence of only one major stratigraphic surface with a downlapping geometry of a maximum flooding surface. This study aims to describe the sedimentary architecture of the shelf-margin slopes and illuminate the possible origin and actual nature of this surface. In addition to 3D seismic interpretation, forward stratigraphic modeling was used to highlight the constraints on slope development. The results from this research can be relevant in lacustrine and marine shelf settings, providing a similar combination of the directionally different, coeval, avulsion-related feeder systems that influenced the progradation of basin margin slopes.

It is worth noting that the research outlined above not only profits from the opulence of the vintage data left from the decades of petroleum exploration but is greatly improved by more recently acquired 3D seismic blocks. It also can give practical results in a better definition of the subsurface geological elements essential for generating and accumulating oil and gas and other geoenery resources. Such a mature petroleum province has been described in the review paper by Velić et al. (2012). The analysis of all the known reservoirs reveals that most of the large oil reservoirs and a good proportion of the gas and gas condensate reservoirs were discovered in the Upper Miocene and Pliocene sandstones with intergranular porosity. The cumulative oil production from these fields (Velić et al. 2012) confirms that the so-called ‘Upper Miocene play’ shall remain a valid exploration target. This was subsequently proven by modeling the remaining hydrocarbon potential for the eastern part of the Drava Basin (Cvetković et al. 2018), East of the studied area, where there are clear indications that even the Pliocene part of the sedimentary sequence is a valid exploration play. Thus, the methodology and results explained in this paper can render applicative results because 3D seismic interpretation and seismic stratigraphy can help explorationist define new, untested prospects within an already proven hydrocarbon play. Nowadays, it is not only the oil and gas exploration that will be important but the future assessment of everything that is put under the common term ‘geoenery’: geothermal potential, geological storage of carbon dioxide, as well as underground storage of hydrogen and underground storage of energy.

Geological setting

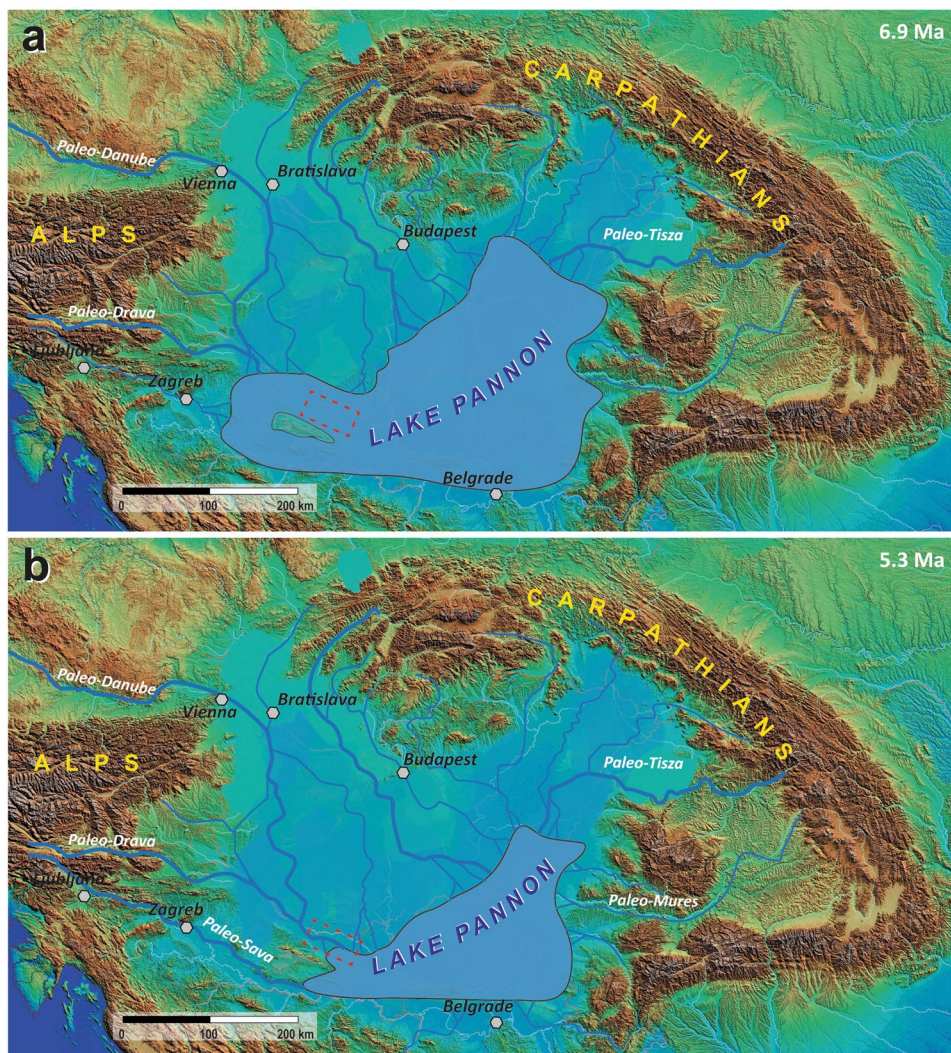
Drava Basin is situated in the SW part of the Pannonian Basin System (Fig. 1a), a large extensional back-arc basin between the Alpine, Carpathian, and Dinaride orogenic belts (Horváth et al. 2006, 2015; Balázs et al. 2016, 2017). Up to 7 km of Neogene to Quaternary deposits were accumulated

above the Palaeogene-Mesozoic basement (Pamić et al. 1995; Horváth et al. 2006; GKRH 2009; Horvat et al. 2018; Cvetković et al. 2019). Extension in the SW part of PBS occurred mainly along extensional detachments (Prelogović et al. 1998; Pavelić 2001; Balázs et al. 2017; Fodor et al. 2021; Nyíri et al. 2021). The formation of the Drava Basin was initiated in the Early Miocene in terrestrial to lacustrine settings (Harzhauser and Mandić 2008), while during the Early to Middle Miocene syn-rift phase, it became part of the Central Paratethys sea (Rögl et al. 1983; Tari and Pamić 1998; Pavelić 2001; Saftić et al. 2003; Sant et al. 2017; Pavelić and Kovačić 2018; Brlek et al. 2020). The subsequent Upper Miocene and Pliocene post-rift sedimentary infill was deposited in the brackish Lake Pannon and the following alluvial environments (Figs. 2, 3; Magyar et al. 1999, 2013; Pavelić and Kovačić 2018; Mandić et al. 2019; Sebe et al. 2020).

The turnover from the marine to the brackish lacustrine setting was associated with regional compressional events, uplifting the central part of the PB, coeval with the subsidence of the marginal areas, as well as increasing uplift of the surrounding orogenic belts, leading to the development of a regional unconformity at the base of the lacustrine strata (Figs. 1c, 4; e.g., Horváth 1995; Horváth et al. 2006; Balázs et al. 2016; Sebe 2021). Another pulse of tectonic inversion caused by the northward shift and rotation of the Adriatic microplate began concurrently in the western part of the PBS at about 8 Ma (Bada et al. 2007; Uhrin et al. 2009). Inversion-related phenomena propagated eastward, and the peak of compression commenced from the end of the Late Miocene onwards (Prelogović et al. 1998; Lučić et al. 2001; Tomljenović and Csontos 2001; Matoš et al. 2016; Balázs et al. 2016). Change in a stress regime caused reactivation of older normal faults as reverse, strike-slip faulting, block rotation, and folding, which led to simultaneous uplifting and active subsidence of regional structural units (e.g., Márton et al. 2002; Jarosinski et al. 2011; Fodor et al. 2021). Due to compressional structural events, another basin-wide unconformity potentially coinciding with the Miocene-Pliocene boundary was recognized on seismic profiles also in the W and NW part of the Drava Basin (Šimon 1973; Sacchi et al. 1999; Saftić et al. 2003; Malvić and Cvetković 2013; Sebe et al. 2020). The correlative conformity can be followed in the Eastern Drava Basin study area as one of the topsets, finally continuing as a clinof orm (Fig. 3; Sebe et al. 2020).

The history of the lacustrine sedimentary fill was reconstructed based on both the surface (Vasiliev et al. 2007; Bakrač et al. 2012; Pavelić and Kovačić 2018 and references therein) and subsurface data (Saftić et al. 2003; Bigunac et al. 2012; Malvić and Cvetković 2013; Kamenski et al. 2020; Sebe et al. 2020 and references therein). Late Middle Miocene to Late Miocene sedimentation might have been continuous in the main depocenters (Pavelić 2001; Kovačić

Fig. 2 Paleogeography of Lake Pannon and the sediment feeder river systems during the latest Miocene **a** and early Pliocene **b** (modified after Sztanó et al. 2020)



et al. 2017), while the basement highs and their environs were flooded by Lake Pannon only a few million years later (Magyar et al. 1999; Uhrin et al. 2009; Sztanó et al. 2013b; Sebe et al. 2020). Accommodation increased due to climatically-induced lake-level rise coupled with basin subsidence, creating water depths up to 1300 m in the central part of the Drava Basin (Kovács et al. 2021). Calcareous marls are intercalated with locally derived coarse-grained gravity-flow deposits in deep central parts of such narrow basins (Figs. 3, 4; Saftić et al. 2003; Sebe et al. 2020).

Meanwhile, the uplift and erosion of the active orogens around Lake Pannon produced a large volume of sediments, which entered the basin via several river systems and filled the lake gradually with turbidites, slope, and deltaic deposits (Figs. 3, 4; e.g., Magyar et al. 1999; Lučić et al. 2001; Kovačić et al. 2004; Juhász et al. 2007; Vrbanac et al. 2010; Sztanó et al. 2013a, b; Bartha et al. 2022; Radivojević et al. 2022). In the zones where the numerous fluvial feeder systems reached the lake, all along the periphery (Fig. 2;

Sztanó et al. 2020), wide ‘morphological shelves’ accreted (cf. Porebski and Steel 2003), continuing in the shelf-slope down to the several hundred-meter-deep lake floors. These slopes were primarily constructed from mudstones, the suspended load of the rivers. The sandy sediments were distributed between the shelf and the deep basin interiors. Sand accumulated in the progradational delta lobes on the shelf and was directly transported to the turbidite systems via the slope when deltas reached the shelf edge. These are today observed as the progradational to aggradational clinof orm system, consisting of topsets, several hundred meters high foresets, and the bottomsets, similar to many marine systems (e.g., Vakarcs et al. 1994; Magyar et al. 2013; Sztanó et al. 2013a, ter Borgh et al. 2014; Sztanó et al. 2016; Magyar 2021; Radivojević et al. 2022). The climate-driven lake-level changes influenced the rate of aggradation to progradation, sand transport and storage, and types of transport processes both on the shelf and the slope (Uhrin and Sztanó 2012; Sztanó et al. 2013a; Gong et al. 2018; Kovács et al. 2021).

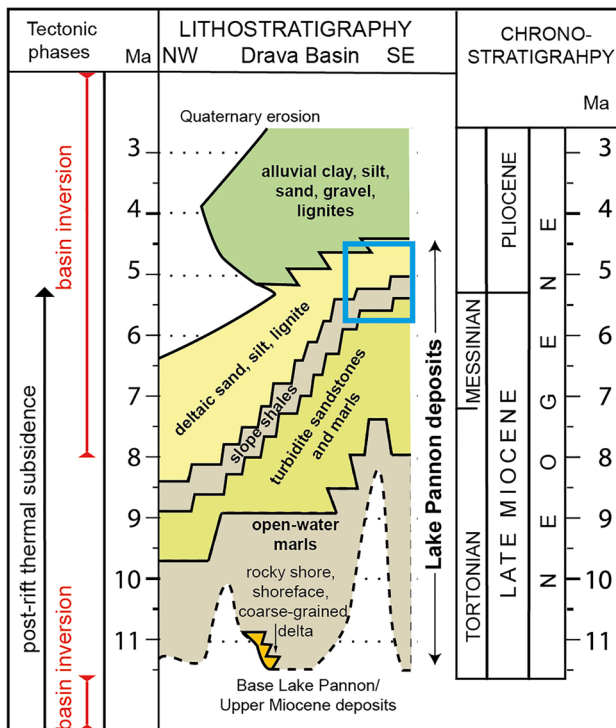


Fig. 3 The lithostratigraphy of lacustrine strata in the Drava Basin with the main tectonostratigraphic events (after Saftić et al. 2003; Balázs et al. 2016; Sebe et al. 2020). This study is focused on deposits marked with the blue rectangle

At about 8 Ma, the shelf edge fed by the paleo-Danube system approached the NW Drava Basin and turned towards the southeast (Sebe et al. 2020). This latter axial system is regarded as the paleo-Drava in this study (Figs. 1b, 2). During more than 3 Ma, the paleo-Danube continuously supplied sediments and built a slope from the north; thus, the junction zone gradually shifted to the east. The repeated confluence of slopes at about 5.3 Ma in the eastern part of the Drava Basin is the subject of this study. Ultimately, Lake Pannon was filled up in the Drava Basin during the Pliocene (Fig. 3; Sebe et al. 2020). The lacustrine environments were transformed into alluvial plains, with relatively small fresh-water lakes to swamps in the southern marginal parts of the PBS (Mandic et al. 2015; Anđelković and Radivojević 2021).

Data and methods

3D and 2D seismic and well data were used to gain insight into the subsurface architecture and stratigraphy (Figs. 1, 3, 4). The data were acquired during the hydrocarbon exploration (<https://www.azu.hr/en>). Data integration and analysis were done using the Schlumberger Petrel E&P software platform. Reflection seismic is displayed in SEG reverse polarity, with red representing the positive polarity. For well-tie

calibration, the checkshots from selected wells were used. Well-to-seismic ties and time-to-depth conversion were done using the three-layered velocity model. After that, original stratigraphic reports were digitized and harmonized to give geological meaning to the selected horizons (Fig. 4).

Main stratigraphic horizons and clinofolds were mapped in an area of more than 600 km². The interpretation was made following the original concept of seismic stratigraphy (Vail et al. 1977) and shelf-edge trajectory mapping (Helland-Hansen and Hampson 2009; Henriksen et al. 2011; Patruno and Helland-Hansen 2018). We interpreted several large- and small-scale clinofolds corresponding to the different stages of basin infill.

Since the succession was post-depositionally deformed and tilted, time-depth maps do not illustrate the contemporary geometry or dip direction of clinofolds. Because structural dip is usually less than 5–10° instead of back-stripping, a less accurate but straightforward method was used to restore the clinofolds (cf. Sztanó et al. 2013a). The original slope surfaces were approximated by thickness maps generated between the clinofolds and the overlying paleo-horizontal, i.e., shelf or delta plain surfaces slightly younger than the clinofolds to be visualized. To follow slope progradation, thickness maps of successive clinofolds were also generated. In both types of thickness maps, the different elements of clinofolds (e.g., top, shelf edge, slope, and bottom) were enhanced by contouring and coloring. The high-resolution shelf-edge geometry, slope surfaces, and trajectory maps (Fig. 5b) were constructed in this way. RMS amplitude maps were also analyzed to visualize sedimentary bodies, e.g., distribution, shape, and orientation of sandy channels or lobes (Fig. 6). While doing so, the closest peak was searched above and below the surface in a window of 40 ms.

The 46 km-long composite seismic section (Fig. 4), primarily parallel with the axis of the Drava Basin, connects the key wells (Čd-1, Mag-2, Sj-2) and provides information on the lithological composition using the spontaneous potential (SP) and resistivity (Ra) logs. Wherever possible, they were controlled by the available gamma-ray, neutron, sonic logs, and mud log data. The volume of the shale (Vsh log) was created using the SP logs as input. Higher values (up to 1) indicate more mud-prone intervals, while the lower (close to 0) mean sand-prone intervals. The master section and well data reveal the local stratigraphic and structural features. The reflection terminations were also interpreted in terms of sequence stratigraphy to reveal controls on the depositional architecture.

A series of numerical experiments have been conducted to better understand the origin of the observed stratal stacking pattern. Forward stratigraphic modeling is an excellent tool for constraining subsurface data interpretation and testing the interaction of different controlling factors. For

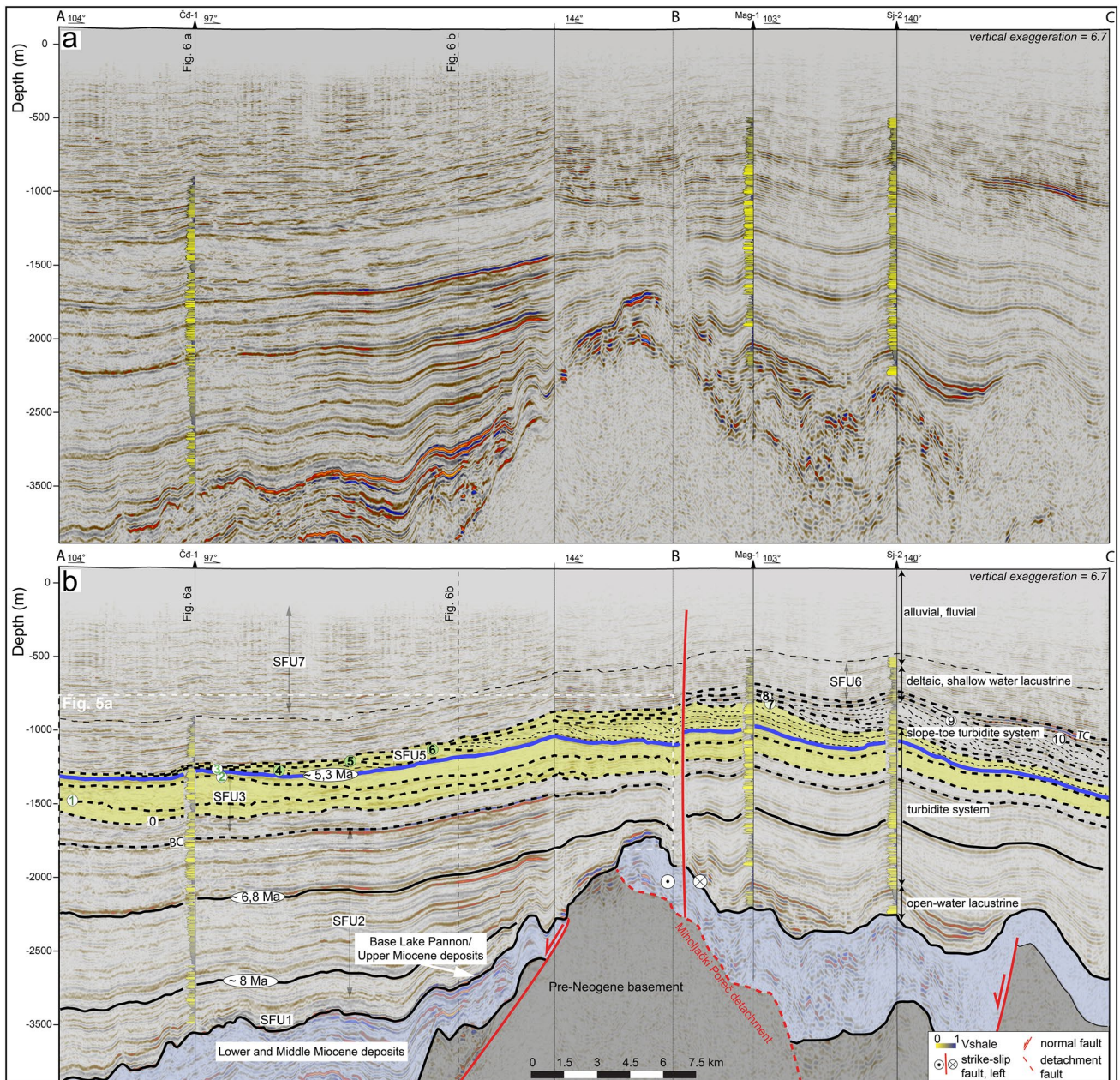


Fig. 4 The uninterpreted **a** and interpreted **b** composite seismic section shows the stratal architecture of the basin fill succession in the Eastern Drava Basin. The large clinoform sets (0–3) are overlain by downlapping small ones (4–6), which were followed by large ones again (7–10). The origin of horizon 3 (solid blue line) is the focus of this study (yellow area, clinoforms in focus). The estimated age data

is based on biostratigraphic interpretation (solid lines, Sebe et al. 2020). Clinoforms are visualized with dashed lines. Vshale is the volume of shale log, wide yellow parts are for sand-prone, and narrow brown parts are for mud-prone lithofacies, respectively. BC base, TC top of clinoform package. For the location, see Fig. 1c

this purpose, we used a diffusion-based numerical forward modeling software called Dionisos (Granjeon and Joseph 1999; Granjeon 2014). The software solves different diffusion equations to simulate the stratigraphic evolution of sedimentary basins over geological time. It considers structural movements, water-level changes, variations in sediment

supply, compaction, and erosion (Granjeon and Joseph 1999; Granjeon 2014).

A 40 × 30 km model domain with a 500 m cell size was created to accommodate the complex geology of the studied part of the Drava Basin. Our main aim was to study the sedimentary response to alternating sediment input directions, variations in water discharge of the source(s), and enable

simulating the switching of the separate active deltaic feeder systems at different time steps.

Results and interpretation

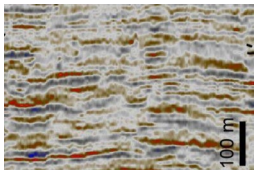
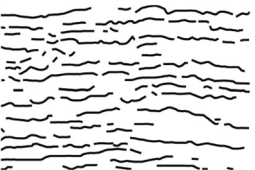
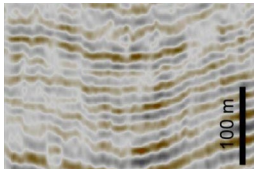

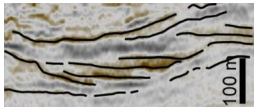

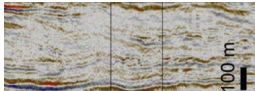

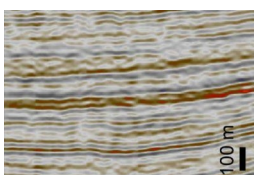
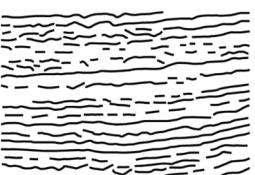
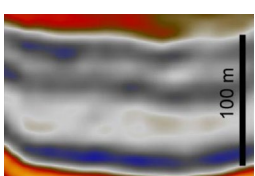
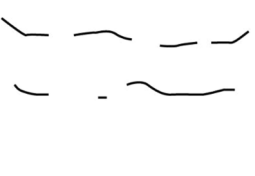
Seismic facies

Six seismic stratigraphic units have been distinguished in the Upper Miocene to Quaternary sedimentary succession (Fig. 4, Table 1). The first two ‘seismic facies units’ (SFU1–SFU2) represent the deep-water Lake Pannon deposits, attaining an overall thickness of 1700 m (in Čď-1 well). This study focuses on the overlying up to 500 m thick series of clinoforms (SFU3 and 4). SFU 5–6 reflect the shallow-water deltaic to alluvial successions, which are 700–1300 m thick in this part of the Drava Basin.

The SFU1 involves reflectors at the bottom of the Upper Miocene lacustrine succession, onlapping on the inverted Middle Miocene or the basement. It is a thin seismic package of subparallel, discontinuous low to high-amplitude reflectors. They represent the calcareous marls sporadically intercalated with coarse-grained clastics (in Mag-1 well). The next unit comprises SFU2, alternation of subparallel, continuous to discontinuous, hummocky and lenticular, low to moderate amplitude reflectors parallel to subparallel, generally continuous, high amplitude reflectors. These units consist of a sequence of clay marls and interfingering sandstones of turbidite systems.

The sigmoidal and oblique reflectors correspond to the clinoforms and are divided into two units: SFU3 and 4. The fairly continuous, sigmoidal, and locally hummocky, medium amplitude reflectors are part of the SFU3. The oblique discontinuous, low amplitude reflectors comprise

Table 1 Description of seismic facies units used in seismo-stratigraphic interpretation

Seismic facies unit	Example from 3D data	Interpretation	Reflection characteristics	General lithology
SFU6			Parallel discontinuous, low to high-amplitude reflectors	Sands, gravels, clays, coal, peat
SFU5			Parallel, relatively continuous, high-amplitude reflectors	Heterolithic facies, silts, sands, clay, coal
SFU4			Oblique discontinuous, low amplitude reflectors	No well data
SFU3			Fairly continuous, sigmoidal, and locally hummocky, medium amplitude reflectors	Mostly clay marls, siltstone, silts, alternation of clays and sandstones, sporadically coal fragments and rarely gravels
SFU2			Alternation of subparallel, continuous to discontinuous, hummocky and lenticular, low to moderate amplitude reflectors with the parallel to subparallel, generally continuous, high amplitude reflectors	Clay marls, marls, and interfingering sandstones of turbidite systems
SFU1			Subparallel, discontinuous low to high amplitude reflectors	Calcareous marls sporadically intercalated with coarse-grained clastics

SFU4. The topsets represent the shelf, the foresets the shelf-margin slope, and the bottomsets the turbidite lobes near the slope. Clinoform 2 is an onlap surface, while clinoform 3 is a low-angle downlap surface overlain by small-scale, i.e., 50–100 m high clinoforms (4–6).

The parallel, relatively continuous, high amplitude reflectors, described as SFU5, correspond to the progressing delta lobes, though their clinoforms are too small to be shown at this resolution. Due to repeated floodings of the shelf, these can be stacked up to 150 m. The subsequent parallel discontinuous, low to high amplitude reflectors represent alluvial plains with fluvial channels of SFU6.

Clinoform progradation in sequence stratigraphic context

Upper Miocene to Pliocene slope progradation can be followed by the clinoform stacking pattern displayed on regional seismic sections through the Drava Basin (Figs. 4, 5, 6; cf. Sebe et al. 2020; Kovács et al. 2021). In addition to clinoforms, and 1–10 surfaces, two horizons marked BC at 1740 m and TC at 1227 m depth of Čd-1 well were also mapped, as two roughly parallel reflectors below and above the clinothems (Figs. 4 and 5). BC is the basin floor continuation of a clinoform far to the west, while TC follows a reflection in the deltaic deposits, which was used

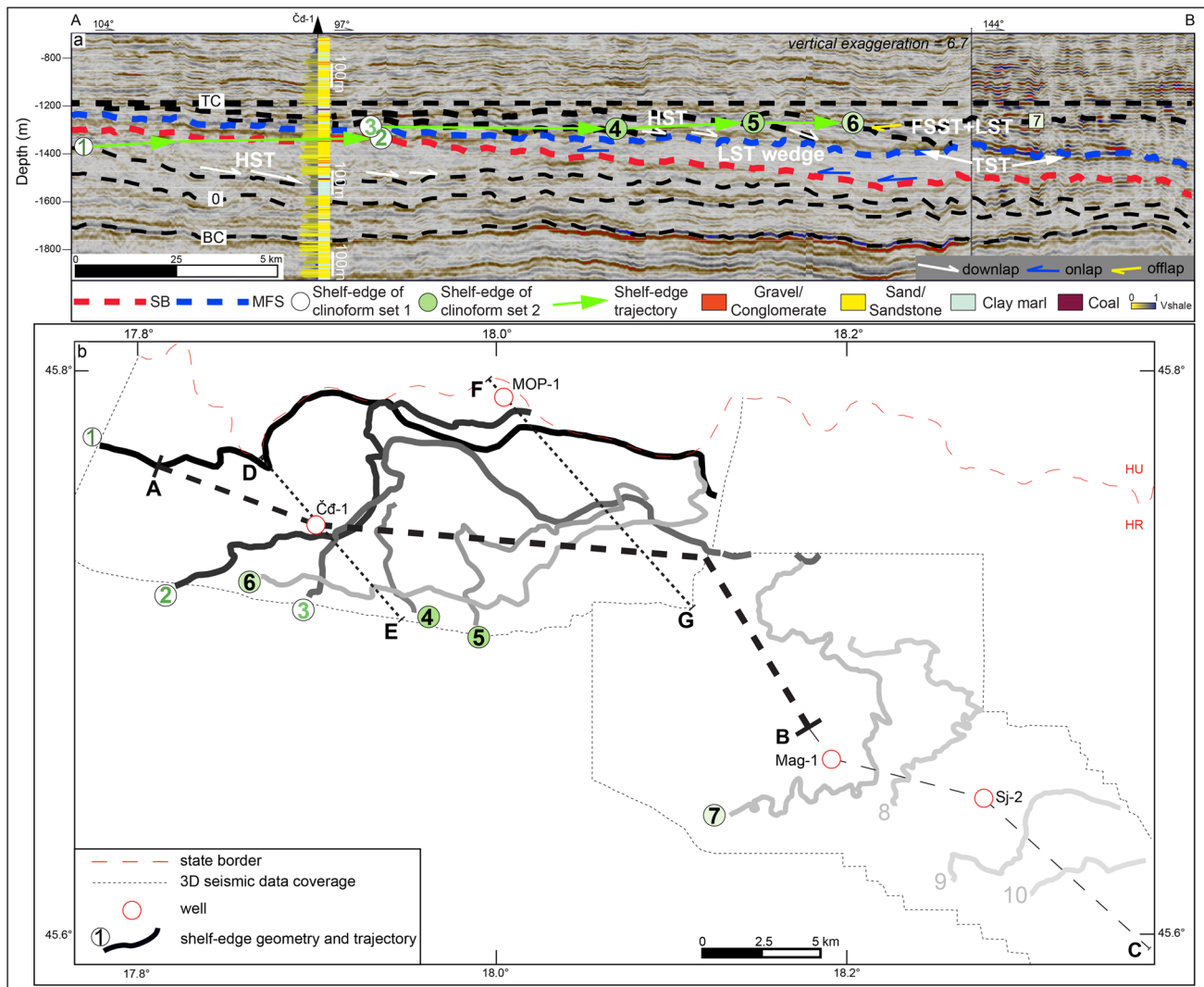


Fig. 5 Progradation of clinoforms in cross-section (a) and map view (b). **a** Clinoforms 1–7, reflection terminations, and sequence stratigraphic interpretation of the section. *SB* sequence boundary, *MFS* maximum flooding surface, *HST* highstand system tract, *TST* transgressive system tract (thickness is below seismic resolution, so represented only by the downlap surface of the *MFS*). **b** High-resolution

map of fore- and locally backstepping shelf-edges of clinoforms younging from 1 to 10. Note complex geometry that indicates the variability of transport directions. The smaller set, starting with clinoform 4, is shown in grey, from the oldest dark grey to the youngest light grey clinoform shelf-edge 10

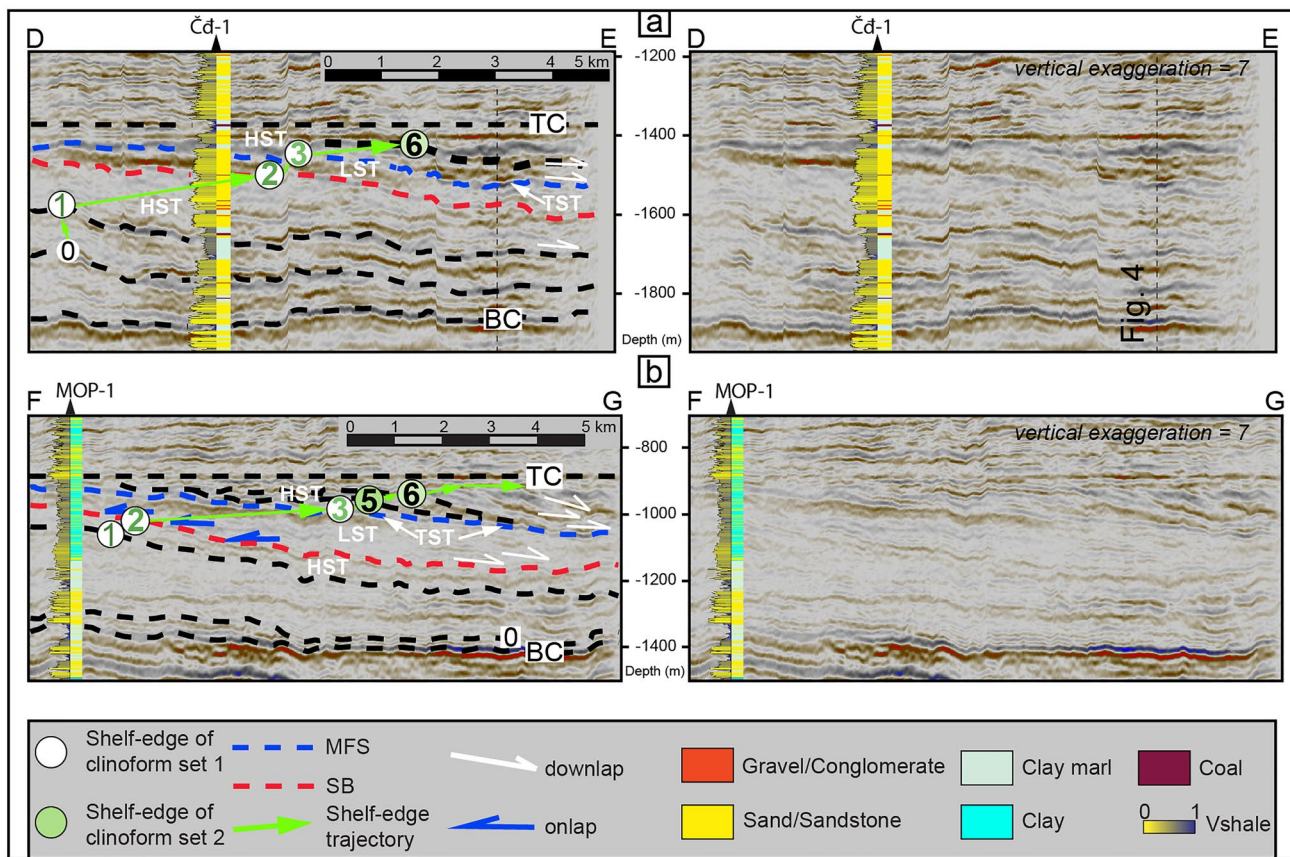


Fig. 6 The two sections illustrate the along-the-strike variability of sedimentary stacking patterns, lithofacies associations, and shelf-edge trajectories of the clinoforms 1–6. *MFS* maximum flooding surface, *HST* highstand system tract, *TST* transgressive system tract (below seismic resolution), *LST* lowstand system tract, *Vshale* the volume of shale. Figures a and b reveal different system tracts along the strike of the shelf edge 1, 2, and 3. For example, a small clinoform set (1–2)

is interpreted to be developed in HST, with forestepping in the D-E section (a), while the same strata in the F-G section (b) have slight backstepping nature. Specifically, clinoform 3 seems to be slightly backstepping in the area of the Čď-1 well (D-E), while it has a strong forestepping, progradational character in the MOP-1 well area (F-G section)

a paleohorizontal proxy. The two generations of clinoforms also give insight into the base-level changes via analysis of the shelf-edge trajectories and reflection terminations (cf. Helland-Hansen and Hampson 2009). The large (0–2) and the small sets (4–7) are separated by clinoform 3. Both clinoform 2 and particularly clinoform 3 show an apparent low dip angle because the cross-section is not in the dip direction of the slope (Figs. 4 and 5.). The reflection terminations highlight their main difference: clinoform 2 is an onlap surface, while clinoform 3 is a downlap surface (Fig. 5a).

The shelf-edge trajectory of clinoforms 1 to 2 is ascending to flat. Above clinoform 3, a forestepping and rising trajectory from 4 to 7 occurs. The clinoform height is gradually increasing to the East from 7 to 10. Finally, they take the sigmoidal geometry and height, similar to the first ones (Fig. 4). According to the succession in the Čď-1 well, below clinoform 0, the thick graded turbidite sandstones and clay marls alternate. These are overlain by a 60 m thick

interval of clay marl, pointing to a longer pause in sediment input, so this interval is interpreted as TST topped with a maximum flooding surface at clinoform 1 (Fig. 5). The clinoforms from 1 to 2 are characterized by downlapping terminations and ascending to flat shelf-margin trajectory. The interval of slope deposits in the Čď-1 well (1550 to 1330 m) reveals sandy slope turbidites. It starts with thin sandstone layers, fragments of coal registered on the mud log, overlain by thick sandstones intercalated with clay marls. Sporadic interlayers of gravel also occur. Coarsening upward units are followed by fining upward ones, with thicknesses from 10 to 25 m, indicating switching of slope lobes. From clinoform 2–3, slope progradation continued south of well Čď-1 and further to the NE, south of well MOP-1, but slope progradation was nearly negligible between these locations. Though amplitudes are very low in this area, and the reflections are discontinuous, subhorizontal onlapping terminations are noticed above clinoform 2 (Fig. 5a). The

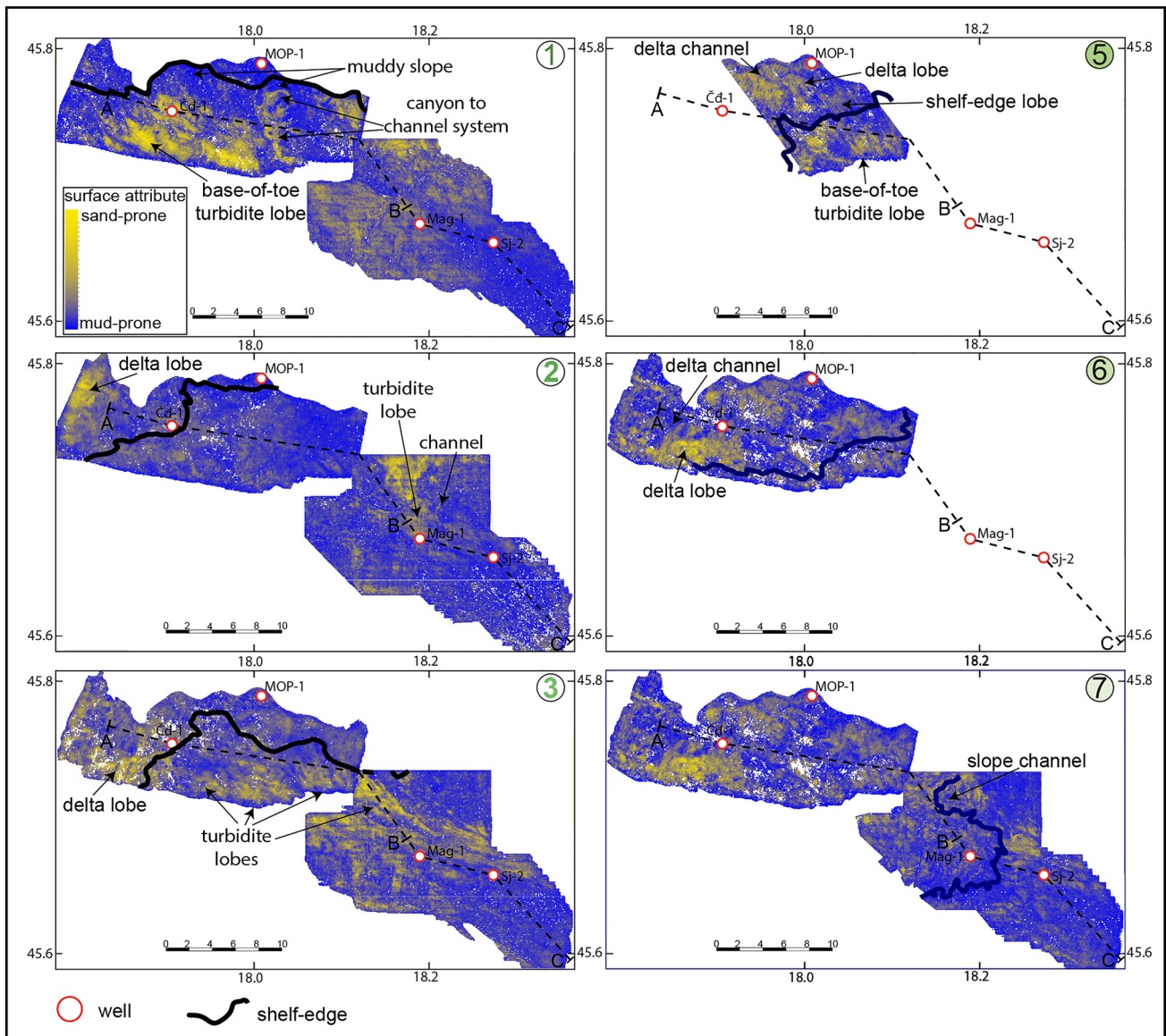


Fig. 7 The RMS maps of clinofolds 1–7 and the position of the related shelf edge. The clinofold 4 was omitted due to too small a surface area. The yellow color indicates more sand-prone, while blue indicates mud-prone lithofacies, thus revealing the geometry of sedi-

mentary bodies. RMS maps show changing sediment dispersal patterns and transport direction across the shelf and basin. These patterns have a different orientation in large clinofolds 1, 2, and 3 (from N–S, NW–SE) and small clinofolds 5–7 (W–E, N–S, NW–SE)

well Čd-1 penetrates thick sandstones in the topset of the corresponding clinothem. These are likely deposits of shelf-edge deltas and mark the end of maximum regression. By combining it with the onlaps, clinofold 2 can be interpreted as an SB and the following clinothem as an LST wedge. At a depth of 1250 m, 10 m thick clay marls overlying the thick sandstones are interpreted as the product of significant flooding, but unfortunately, the seismic resolution does not distinguish MRS/FS at its base, and MFS at its top as separate surfaces. Thus clinofold 3 could be interpreted as an MFS (Figs. 5a, 6a), which is further justified by downlaps of the small clinofold set (4–6 in Figs. 4 and 6). The

toplap and offlap terminations below the TC surface are also visible. The trajectory is flat to rising. The clay marls are overlain by sandstone, with intercalation of gravels at the top; the Vshale log shows a coarsening upward trend (at 1230 m depth of Čd-1 on Fig. 5). The following succession, up to 900 m of depth in Čd-1, is composed of an alternation of sands, sandstones, and clayey marls, with interlayers of gravels and coal beds, representing repeated flooding of the shelf and reappearance of delta lobes at several times. Clay marls, sands, gravels, and lignites with fining upward sand bodies are interpreted as fluvial deposits (above 800 m in Čd-1 well, Figs. 4 and 5a).

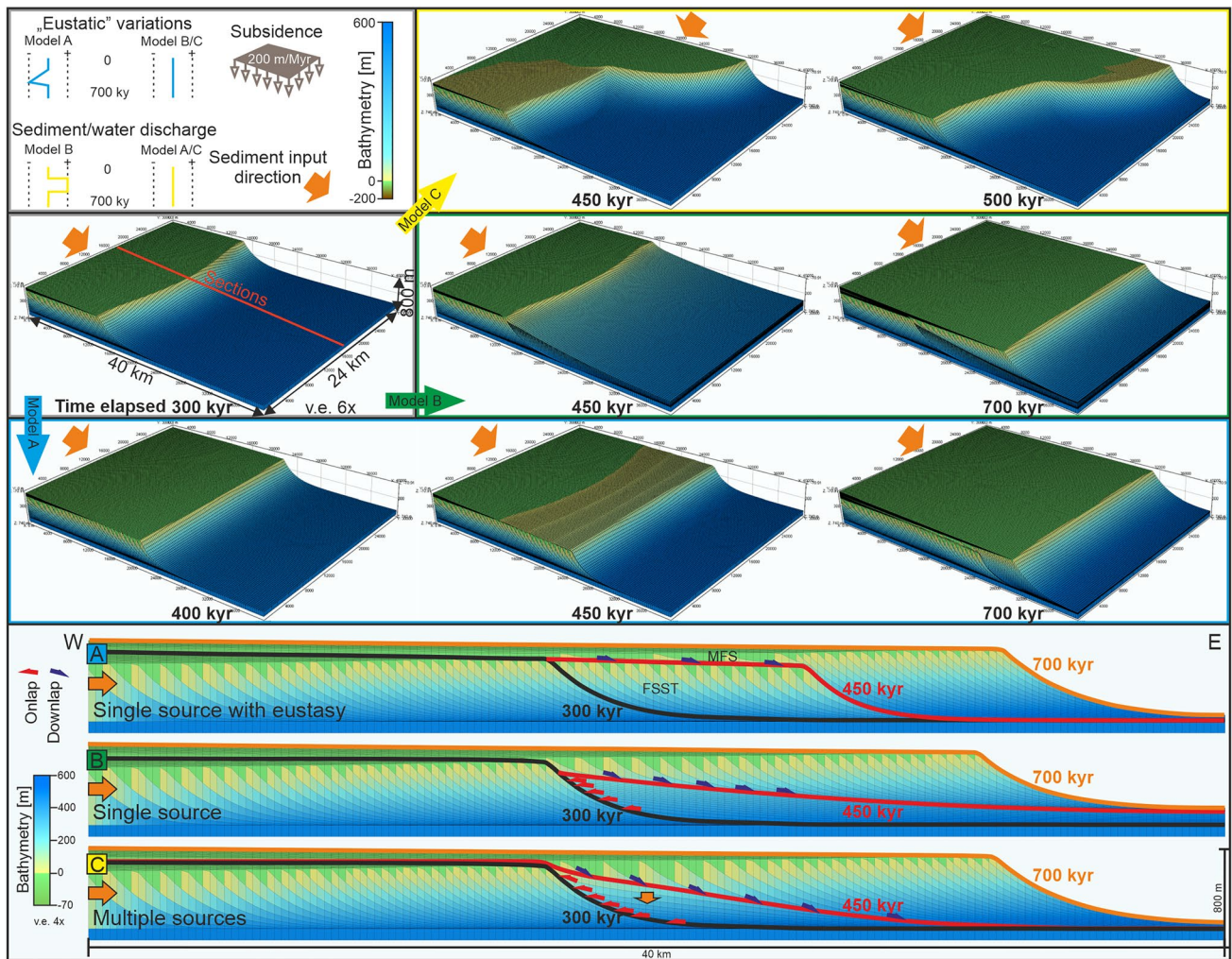


Fig. 8 Testing simplified conceptual models as the origin of the observed stratal stacking pattern. In model A, ‘eustatic’ i.e., water-level variations, are the foundation of the variability. In model B, the

water discharge of a single source varied over time, while in model C, multiple sources with different directions were imposed

Clinothems 4–6 represent the HST. The western part of clinothem 7 shows offlaps followed by flat to rising clinofolds towards SE. Thus, it may represent a minor base level fall to rise, i.e., falling stage system tract and lowstand system tract (FSST + LST).

The studied interval, which displays several 100 ka-long history of slope progradation, comprises two 4th-order depositional sequences (cf. Vakarcz et al. 1994; Sztanó et al. 2013b; Kovács et al. 2021). It shows a slow but continuous, moderate amplitude base-level rise balanced by sediment input, leading to long-term normal regression. Elsewhere in the basin, the 4th-order sequences are manifested as aggradational to progradational shelf-slope cycles (Sztanó et al. 2013a), without seismically mappable fall of base level (e.g., offlaps or onlaps) or sudden change of clinofold height. Other features were detected: a low-angle onlap surface (i.e., an SB overlain by an LST wedge) and a composite downlap

surface overlain by small to growing clinofolds of the following HST. The thickness of TST clays is below seismic resolution.

High-resolution shelf-edge trajectory map and RMS maps

The complex geometries from the oldest clinofold 1 to the youngest 10 are visible on the shelf-edge trajectory map (Figs. 5b and 7). Shelf edges of clinofolds 1–3 and 6–10 were mapped across the 3D volumes up to a distance of 46 km. Spatially uneven shelf-edge geometries characterize both sets of the clinofolds. Some of the long shelf edges show simultaneous forestepping (NW–SE) and backstepping (NW to SE) segments (Fig. 5b). While progradation attains up to 5 km locally, backstepping is only a few hundred meters (1–2, Fig. 5). The sediment transport directions

are indicated not only with the shift of shelf edges but also by the general change in orientation of shelf-edge delta lobes and distributary channels from NW towards SE, as illustrated on RMS maps (Figs. 5b and 7).

The shelf edge of small clinoform 4 is 5 km long, localized only in front of the N-S segment of edge 3 with a forestepping of 3 km towards E. The direction of sediment transport from the western edge segment 1–4 changed by approximately 80°. Shelf edge 5 covers a greater length. It consists of the N-S segment prograding 3 km, while simultaneously, its NE part remained steady with a minor local backstepping behind the shelf edge of clinoform 3. The edge of clinoform 6 shows a markedly different orientation: its eastern segment continued migration towards SE. In contrast, an 11 km long W-E trending segment stepped over all the others with a southward transport direction (all in Fig. 7, small inserted maps are marked with numbers that correspond to the described clinoforms and their shelf edges).

Unfortunately, the mapping of shelf edges was somewhat limited at the junction of the two 3D seismic volumes. The next shelf-edge 7 advanced more than 20 km to the SE and showed a highly arcuate shape of approx. 10 km wide and 7 km long. Edge 8 continued forestepping to the East, roughly 3 km, with a similar lobate shape. The shelf edges 9 and 10 advanced and rotated approximately 45° in the SE direction (SW of S_j-2 in Fig. 5b).

Forward stratigraphic modeling: tests of climate change, sedimentation rate, and sediment source directions

The observed clinoform stacking pattern (Figs. 5a, 6) in the 2D view leaves room for alternative interpretations. We present three model scenarios in Fig. 8 where similar geometries formed due to strikingly different geological processes. The first 300 kyr is identical in every model during which the slope system progrades at a 50 km/Myr rate with a dip angle of 6–9° (Fig. 8). This is comparable to the observed slope angles and progradation rates in the Drava Basin and other subbasins in western parts of the PBS (Magyar et al. 2013; Balázs et al. 2018).

Eustatic variations produced the stratal stacking pattern in Model A with constant sediment supply and input directions. During model time 300–450 kyr, a gradual lake-level drop of 100 m (Fig. 8) resulted in offlaps and a low-angle composite surface of the shelf. The subsequent base-level rise at 450 kyr with a rate of 100 m/100 kyr resulted in the downlapping small clinoform package deposition on top of the shelf.

Model B also has only a single (Western) source. Between 300 and 450 kyr, the water discharge of the external source increased drastically (from 200 to 1000 m³/s) in the model. Compared to the present-day water discharge of the Drava River (500–600 m³/s) (Bonacci and Oskoruš 2010), these

values are reasonable. Since in Dionisos, the transport capacity of the water flow is proportional to the local slope and water discharge (Gvirtzman et al. 2014), increasing the water discharge results in a lower angle local slope. From 450 kyr onward, the water discharge reverts to the original value, creating the downlapping clinoform package on top of the gently dipping strata.

In model C, between 300 and 450 kyr, a 90° switch of the sediment source direction occurred: the West to East system stops, while a North to South sediment source is activated. Section C (Fig. 8) is parallel with the dip of the old slope but displays the new slope in the strike direction. The sudden change is depicted by a series of gently dipping slope surfaces (2–3°) onlapping on the old slope. At 450 kyr, the western source becomes active again, resulting in the deposition of a smaller downlapping clinoform package gradually increasing in size to the East.

Discussion

Our experimental models provide possible explanations for forming the observed stratal architecture. In model A, if the subsequent base-level rise from 450 to 700 kyr has a slow pace relative to the sediment input, it results only in onlaps above the shelf, with progradational to aggradational clinoforms of the LST. If a rapid, high amplitude base-level rise occurs, like in our case (Fig. 8), onlaps are shifted far towards the source area, and without the development of an LST wedge, small downlapping clinoforms mark the TST above the composite offlap surface. However, this simple scenario does not reproduce the observed low-angle surface with the downlapping clinoforms.

By increasing the water discharge due to high precipitation events or the sudden increase in the catchment area, we could reproduce a geometry similar to the observations in model B. The onlapping low-angle surface is the new stable slope profile. However, from a geological perspective, the dip angle of the slope is mainly controlled by other factors, such as the lithology and grain size distribution along with the sediment influx (e.g., Gvirtzman et al. 2014). Such change would only be plausible if tectonic movements in the catchment area caused drastic changes. In the case of the Drava Basin, a regional unconformity is known in the northwest part of the Drava Basin (Saftić et al. 2003; Sacchi et al. 1999; Sebe et al. 2020). This tectonic event in the hinterland can roughly be coeval with the lobe switching events described in this study. Seismic resolution and correlation allow the assumption that clinoform 3 corresponds to correlative conformity described in Sebe et al. (2020). The initial uplift and erosion of former basin-fill successions might have contributed to the variation of sediment input and triggered the avulsion of the northern delta system. It also could

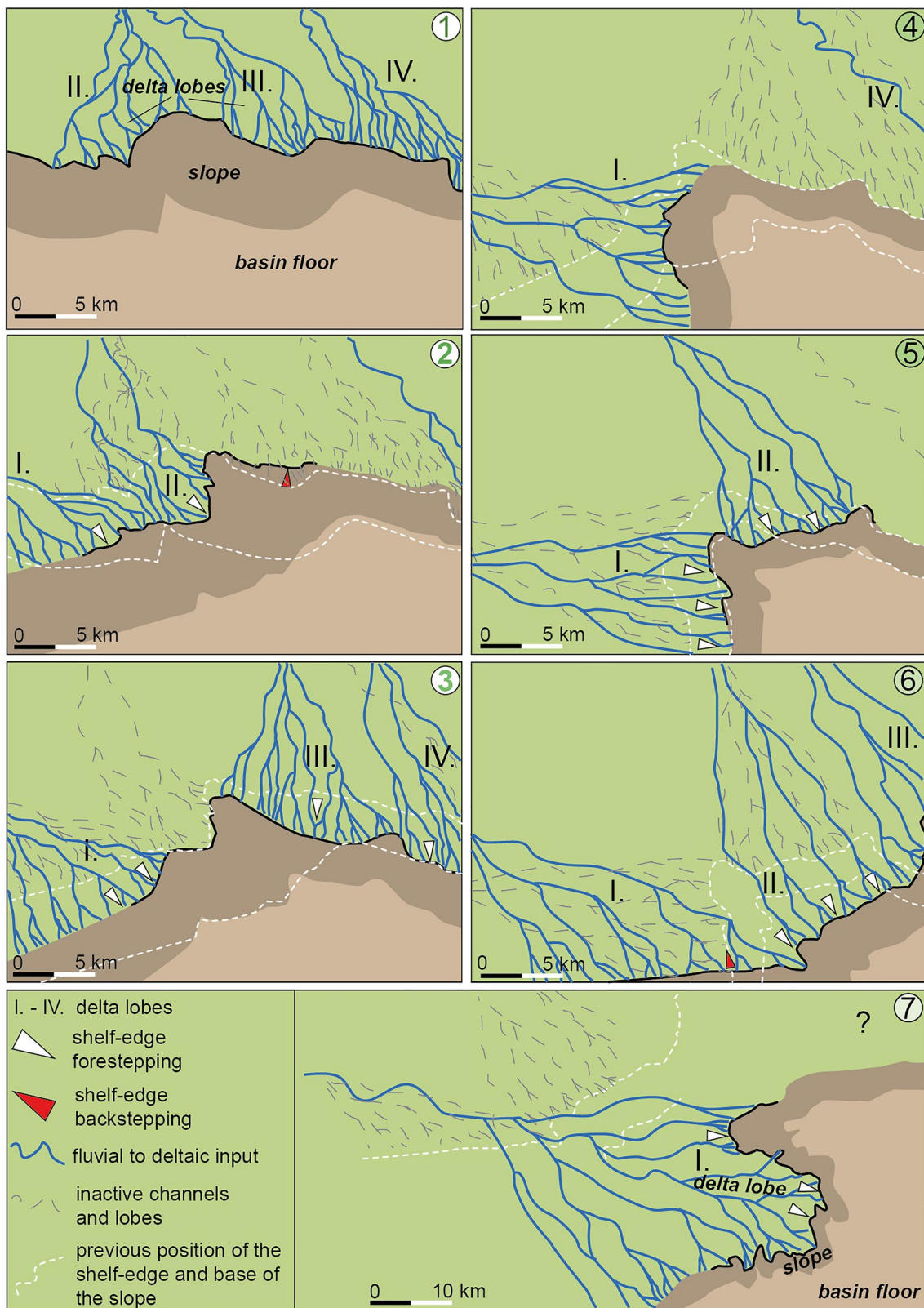


Fig. 9 The conceptual cartoon shows the evolution of fluvial to deltaic feeders and the related slopes. The numbering of snapshots corresponds to the clinoforms 1–7 and their subsequent development: large sigmoidal clinoforms (1–3) with two segments, as the Paleo-Danube prograded from the N to S and the Paleo-Drava from NW to

SE. The small oblique clinoform (4) indicates the infill of the embayment between the two major systems. Development of 5 and 6 marks activity of both the northerly and westerly feeder systems. Finally, the large clinoform (7) continues to prograde towards SE in the eastern part of the study area. To be compared with Figs. 5 and 7

have contributed to its eastward shift. However, a change in subsidence rates on a 5 km scale is not likely. Also, we would expect a gradual transition in the slope angles marked by the erosion of the old slopes. These events would also have other effects, such as a lake-level rise marked by coeval aggradation, which we do not see in the study area. Therefore, model B cannot geologically explain the formation of the aforementioned low-angle surface.

The temporal change in the deltaic feeder system directions in model C is in concordance with the results of the mapped shelf-edge trajectory (Fig. 5), which suggest non-uniform shelf-edge migration (cf. Helland-Hansen and Hampson 2009). Both simultaneous backstepping, steady state, and different rate forestepping of shelf-edges occurred (Fig. 5). Possible sequence of events/palaeogeographic changes is illustrated in Fig. 9. For instance, migration from clinof orm 1–2 occurred basinward up to 5 km distance at the western part (lobes I and II), with a coeval retreat in the area of MOP-1 well (Figs. 5 and 7). This backstepping did not mean the destruction of the shelf edge, as it was accompanied by the minor rise of the trajectory (Fig. 6), i.e., of the base level rise of the HST. Therefore, both the progradation and the retrogradation occurred when accommodation increased; the western segment was overwhelmed by sediment input. Meanwhile, sediment input did not keep up with the rise to the east. Probably an avulsion of the deltaic feeder system (II) occurred, and the channels of the area became inactive. With this, approx. 5 × 5 km large embayment of the shelf-slope developed. The situation from clinof orm 2 to 3 was even more complicated. Lake level rose (approx. 30 m, measured without decompaction), and two different input systems can be recognized at the SW and NE corners of the study area. The southwestern one (I) gradually produced less progradation towards Čď-1, with stagnation NE from Čď-1 (Fig. 5b). Thus, minor revitalization of the abandoned northerly feeder system (II) occurred. However, the major input shifted to lobes III and IV further East (approx. 10 km long). The lobe II was not active, while the most eastern segments, lobes III and IV, had enough sediment supply for progradation. It reflects along-strike variability of the sediment input rates on a 5 km scale, illustrating the model example of Kovács et al. 2021 (compare Figs. 7 and 9).

The clinof orm 4 marks a short time interval when the only active lobe in the 3D seismic area was the western source (I, Fig. 9). The western system prograded up to 3 km into the basin, filling the accommodation above surface 3 during the HST, perpendicular to the previous pattern during the deposition of clinof orms 2–3. According to the seismic data, an avulsion of northern systems II, III, and IV happened again, perhaps switching further to the E. In addition, clinof orm 4 shows a character of delta to slope transition (cf. Sztanó et al. 2015). The northern system II was reactivated again from clinof orms 4 to 5, resulting in simultaneous

progradation and further filling of the embayment (also in Fig. 5b). Both the western and northern feeder systems prograded further to the SE from clinof orms 5–6. The embayment in the mapped seismic area was filled with lobes I and II and reactivated lobe III on the scale of 10 km. Particularly, lobe I rotated more to the S, filling the W-E segment of the shelf-edge, while lobes II and III prograded towards the SE (Fig. 5b). The following clinof orm 7 marks the period of lake level fall of approx. 60 m (FSST + LST). The western feeder system prograded 20 km to the SE. At the same time, there is no sign of lobes of the northern feeder system in the seismic area (Figs. 5b, 7). The RMS pattern in Fig. 7 leaves a possibility to speculate if, again, an avulsion and migration of the northern system caused the creation of a new embayment to the north of the lobe I and Mag-1 well area (Fig. 5). The hydrographic reorganization could be directed by the morphology of the basin depocenter. However, this cannot be validated without the data on the syn-sedimentation basin morphology, which was outside the scope of this research.

Along-strike irregular systems of lacustrine and marine deposits can be explained by changing locations of sediment input (e.g., Kovács et al. 2021) and with ‘hinge’ models (Madof et al. 2016). The hinge point is where ‘retrogradational and progradational successions’ are separated (Zecchin and Catuneanu 2020). Both studies above (Madof et al. 2016; Zecchin and Catuneanu 2020 and references therein) corroborate the conceptual models of the along-strike variability and laterally discontinuous bounding sequence stratigraphic surfaces. Madof et al. (2016) proposed a: (i) fixed (accommodation space related to tectonic tilting, shallow faulting, and differential compaction on a scale of 30 km) and (ii) moving hinge models (10 km scale, lateral accommodation space related to the shift of hinterland uplift, along strike relative sea level and water depth variability). The latter model is more prone to record the along-strike variability (Madof et al. 2016). Moreover, in a review article by Zecchin and Catuneanu (2020), the authors relate the origin of the ‘stratigraphic hinge’ to numerous processes which could apply to our study area, such as the high frequency of base-level changes, variability of sediment supply and budget, local tectonism, and physiography. The avulsion of sediment input, i.e., the activation of different lobes (I–IV) within the western and northern feeder systems, could be explained by any of the above-forcing factors.

For instance, climate-induced high-frequency lake-level changes can lead to lateral depositional variability (cf. Kovács et al. 2021). The Lake Pannon water-level fluctuation depended on relatively dry and humid climatic variations (Uhrin and Sztanó 2012) or, in other words, on the humid and less humid periods (Gong et al. 2018). Sediment dispersal patterns and bypassing in the deep basin were related to the hyperpycnal flows occurring during the lake level rise in more humid periods (Gong et al. 2018).

Thus, the variable sediment entry points and coeval retrogradation and progradation seen in our data can be related to high-frequency changes in lake level.

The analyzed clinof orm stacking and reflection terminations could give insights into the architecture of fourth-order sequences (cf. Vakarc s al. 1994; Sztanó et al. 2013a). Depending on the lateral extent, the high-frequency auto cycles could also contribute to the generation of continuous or discontinuous stratigraphic surfaces (Zecchin and Catuneanu 2020). In that instance, the top of the abandoned lobes can be an apparent MFS (Catuneanu et al. 2009). It is plausible that this is the origin of the wide clinof orm 3 (MFS/MRS) since the interplay of active and inactive individual lobes (I–IV, Fig. 9) visible in the seismic can produce local downlapping stacking patterns. Thus, we hypothesize strictly local sequence stratigraphic implications of the clinof orm 2 and 3 (Fig. 7).

Non-uniform shelf-edge migration is the most spectacular feature at the turn of the Miocene to Pliocene in the Drava Basin. At least two different scale mechanisms could trigger the variability of sediment input. The first is an avulsion of major deltaic distributaries and lateral lobe switching related to a single (i.e., Paleo-Danube) feeder system. Irregular migration of the shelf-slope observed in the NW Drava Basin and elsewhere in the PBS was explained this way (Mattick et al. 1985; Uhrin et al. 2009; Sztanó et al. 2020; Fig. 9). Recent examples of depocenter switching (up to 200 km due to the frequently changing base level, high sedimentation, and subsidence rate) in similar systems are reported at the Volga delta in the Caspian Sea (Overeem et al. 2003; Kroonenberg et al. 2005). Among many other examples, delta lobe switching is documented at the Po delta in the Adriatic Sea (Correggiari et al. 2005) and the Danube delta in the Black Sea (Giosan et al. 2005). These results complement the high-frequency water-level oscillations caused by variations between the warm, humid, and arid periods in Lake Pannon (Utescher et al. 2017; Joniak et al. 2020; Baranyi et al. 2021; Šujan et al. 2020 and references therein).

Another possible explanation for non-uniform migration may be the merge of slopes fed by the two different river systems, i.e., the Paleo-Drava and the Paleo-Danube rivers (Magyar et al. 2013; Sztanó et al. 2020). A somewhat similar dynamic was observed in the eastern part of the PBS, where the slopes of the Paleo-Danube and Paleo-Tisza shelves united (Magyar and Sztanó 2008; Vági et al. 2019), although the direction of sediment transport in those cases was almost the opposing one. The distinction of profoundly different feeder systems can be helped by provenance studies of core data in wells from the Drava Basin (cf. Kovačić et al. 2011; Grizelj et al. 2016).

Conclusions

- The enclosed lacustrine systems of Lake Pannon in the Drava Basin are an excellent example of non-uniform shelf-edge migration on a few km to tens of km scale.
- The geometry of progradational shelf-edges and related clinof orms determined by fluvial to deltaic sediment input can be very complex. Avulsions of delta lobes cause along-strike variation in sediment input rates. Thus, shelf slope progradation, stagnation, and retrogradation occur coevally on a scale of km to tens of km.
- Clinof orms reflecting progradational slopes commonly cover other stagnant, oblique slope segments by onlaps, resembling the geometry of sequence boundaries.
- Progradation over stagnant slope surfaces can also produce downlaps, interpreted as apparent MFS.
- The origin of the above stratal architecture was tested with stratigraphic forward modeling. It shows that similar onlap and downlap surfaces can be generated by sudden base-level, sediment, and water discharge changes and along-strike alternation of the two sediment input systems.
- If 2D data is available only, it is impossible to determine which control is of prime importance. 3D data is necessary to detect along-strike variability of the sediment input.
- Autocyclic processes like avulsion and lobe switching controlled complex infilling processes in the enclosed Lake Pannon. High-frequency lake level changes probably enhanced these.
- Shelf-edge trajectory analyses plausibly explain the history of base-level changes. However, the bounding surfaces of onlaps and downlaps can lead to misinterpretation.
- The practical application of this model is of great importance since understanding the role of strike variability promotes the correlation of reservoirs or muddy caprocks at a much more detailed scale.

Acknowledgements The Croatian Hydrocarbon Agency (<https://www.azu.hr/en>) and the Croatian Ministry of Economy, Entrepreneurship, and Craft are acknowledged for providing the seismic and well data used in the study. The authors are grateful to all colleagues who made important geological analyses and valuable results from well data over several decades of O&G exploration in the Drava Basin. The contribution and help of David Rukavina with the syn-rift tectonostratigraphic interpretation were highly valuable. We appreciate help from Vlatko Brčić, Tomislav Kurečić, and Krešimir Petrinjak in proofreading, discussion, and results visualization. We also acknowledge Beicip-Franlab (www.beicip.com) for providing an academic license for DionisosFlow and CougarFlow. The data analyzes were carried out using the academic licenses of the Petrel E&P software platform from Schlumberger. We thank AspenTech Subsurface Science & Engineering for providing Aspen SKUA license as part of the AspenTech SSE academic program. The research was partly financed by the Tempus Foundation

(MŠ) promoting mobility and knowledge exchange between institutions. This paper is also partly the result of training and education conducted through the GeoTwinn project that has received funding from the European Union's Horizon 2020 research and innovation program under grant agreement no. 809943 (MŠ). The Croatian Science Foundation partly supported this work under the project «GEOlogical characterization of the Eastern part of the Drava Depression subsurface intended for the evaluation of Energy Potentials» (UIP-2019-04-3846). National Research, Development and Innovation Office (NKFI) project no. 116618 supported work by ÁK and OSz.

Author contributions MŠ: Conceptualization; Data curation; Formal analysis; Investigation; Methodology; Project administration; Resources; Software; Supervision; Validation; Visualization; Writing—original draft, Writing—review & editing. ÁK: Data curation; Formal analysis; Investigation; Methodology; Software; Writing—review & editing. BS: Corresponding author; Formal analysis; Validation; Supervision; Writing—review & editing. OS: Conceptualization; Validation; Supervision; Formal analysis; Writing—review & editing. All authors read and approved the final manuscript.

Funding The research was partly financed by the Tempus Foundation (MŠ). This paper is also partly the result of training and education conducted through the GeoTwinn project that has received funding from the European Union's Horizon 2020 research and innovation program under grant agreement no. 809943 (MŠ). The Croatian Science Foundation partly supported this work under the project «GEOlogical characterization of the Eastern part of the Drava Depression subsurface intended for the evaluation of Energy Potentials» (UIP-2019-04-3846). Work by ÁK and OSz was supported by National Research, Development, and Innovation Office (NKFI) project no. 116618. Tempus Közalapítvány, AK-00243-004/2019.

Data availability The dataset used for this research can be used with the permission of the Croatian Hydrocarbon Agency (<https://www.azu.hr/en>).

Code availability Not applicable.

Declarations

Conflict of interest The authors declare no Conflicts of interest/Competing interests.

Open Access This article is licensed under a Creative Commons Attribution 4.0 International License, which permits use, sharing, adaptation, distribution and reproduction in any medium or format, as long as you give appropriate credit to the original author(s) and the source, provide a link to the Creative Commons licence, and indicate if changes were made. The images or other third party material in this article are included in the article's Creative Commons licence, unless indicated otherwise in a credit line to the material. If material is not included in the article's Creative Commons licence and your intended use is not permitted by statutory regulation or exceeds the permitted use, you will need to obtain permission directly from the copyright holder. To view a copy of this licence, visit <http://creativecommons.org/licenses/by/4.0/>.

References

- Andelković F, Radivojević D (2021) The Serbian Lake Pannon formations—their significance and interregional correlation. *Geološki Anali Balkanskog Poluostrva* 82(2):43–67. <https://doi.org/10.2298/GABP210420007A>
- Bada G, Horváth F, Dövényi P, Szafián P, Windhoffer G, Cloetingh S (2007) Present-day stress field and tectonic inversion in the Pannonian basin. *Glob Planet Change* 58(1–4):165–180. <https://doi.org/10.1016/j.gloplacha.2007.01.007>
- Bakrač K, Koch G, Sremac J (2012) Middle and Late Miocene palynological biozonation of the southwestern part of Central Paratethys (Croatia). *Geol Croat* 65(2):207–222. <https://doi.org/10.4154/GC.2012.12>
- Balázs A, Matenco L, Magyar I, Horváth F, Cloetingh S (2016) The link between tectonics and sedimentation in back-arc basins: New genetic constraints from the analysis of the Pannonian Basin. *Tectonics* 35:1526–1559. <https://doi.org/10.1002/2015TC004109>
- Balázs A, Burov E, Matenco L, Vogt K, Francois T, Cloetingh S (2017) Symmetry during the syn- and post-rift evolution of extensional back-arc basins: the role of inherited orogenic structures. *Earth Planet Sci Lett* 462:86–98. <https://doi.org/10.1016/j.epsl.2017.01.015>
- Balázs A, Magyar I, Matenco L, Sztanó O, Tókécs L, Horváth F (2018) Morphology of a large paleo-lake: analysis of compaction in the Miocene–Quaternary Pannonian Basin. *Glob Planet Change* 171:134–147. <https://doi.org/10.1016/j.gloplacha.2017.10.012>
- Baranyi V, Bakrač K, Krizmanić K, Botka D, Tóth E, Magyar I (2021) Paleoenvironmental changes and vegetation of the Transylvanian Basin in the early stages of Lake Pannon (late Miocene, Tortonian). *Rev Palaeobot Palynol*. <https://doi.org/10.1016/j.revpalbo.2020.104340>
- Bartha IR, Botka D, Csoma V, Katona TL, Tóth E, Magyar I, Silye L, Sztanó O (2022) From marginal outcrops to basin interior: a new perspective on the sedimentary evolution of the eastern Pannonian Basin. *Int J Earth Sci* 111:335–357. <https://doi.org/10.1007/s00531-021-02117-6>
- Bigunac D, Krizmanić K, Sokolović B, Ivaniček Z (2012) Pyroclastic flow sediment (ignimbrite) in Miocene Tar formation, Drava depression. *Nafta* 9(10):307–314
- Bonacci O, Oskoruš D (2010) The changes in the lower Drava River water level, discharge and suspended sediment regime. *Environ Earth Sci* 59:1661–1670. <https://doi.org/10.1007/s12665-009-0148-8>
- Briek M, Kutterolf S, Gaynor S, Kuiper K, Belak M, Brčić V, Holcová K, Wang LK, Bakrač K, Hajek-Tadesse V, Mišur I, Horvat M, Šuica S, Schaltegger U (2020) Miocene syn-rift evolution of the North Croatian Basin (Carpathian–Pannonian Region): new constraints from Mts. Kalnik and Požeška gora volcaniclastic record with regional implications. *Int J Earth Sci* 109:775–2800. <https://doi.org/10.1007/s00531-020-01927-4>
- Burgess MP, Prince DG (2015) Non-unique stratal geometries: Implications for sequence stratigraphic interpretations. *Basin Res* 27:351–365. <https://doi.org/10.1111/bre.12082>
- Catuneanu O, Zecchin M (2016) Unique vs. non-unique stratal geometries: relevance to sequence stratigraphy. *Mar Pet Geol* 78:184–195. <https://doi.org/10.1016/j.marpetgeo.2016.09.019>
- Catuneanu O, Abreu V, Bhattacharya JP, Blum MD, Dalrymple RW, Eriksson PG, Fielding CR, Fisher WL, Galloway WE, Gibling MR, Giles KA, Holbrook JM, Jordan R, Kendall CGSTC, Macurda B, Martinsen OJ, Miall AD, Neal JE, Nummedal D, Pomar L, Posamentier HW, Pratt BR, Sarg JF, Shanley KW, Steel RJ, Strasser A, Tucker ME, Winker C (2009) Towards the standardization of sequence stratigraphy. *Earth-Sci Rev* 92:1–33. <https://doi.org/10.1016/j.earscirev.2008.10.003>
- Correggiari A, Cattaneo A, Trincardi F (2005) The modern Po Delta system: lobe switching and asymmetric prodelta growth. *Mar Geol* 222–223:49–74. <https://doi.org/10.1016/j.margeo.2005.06.039>

- Cvetković M, Emanović E, Stopar A, Slavinić P (2018) Petroleum system modeling and assessment of the remaining hydrocarbon potential in the eastern part of Drava depression. *Interpretation* 6:11–21. <https://doi.org/10.1190/INT-2017-0078.1>
- Cvetković M, Matoš B, Rukavina D, Kolenković Močilac I, Saftić B, Baketarić T (2019) Geoenery potential of the Croatian part of Pannonian Basin: insights from the reconstruction of the pre-Neogene basement unconformity. *J Maps* 15(2):651–661. <https://doi.org/10.1080/17445647.2019.1645052>
- Fodor L, Balázs A, Csillag G, Dunkl I, Héja G, Jelen B, Kelemen P, Kövér S, Németh A, Nyíri D, Selmeczi I, Trajanova M, Vrabec M (2021) Crustal exhumation and depocenter migration from the Alpine orogenic margin towards the Pannonian extensional back-arc basin controlled by inheritance. *Glob Planet Change*. <https://doi.org/10.1016/j.gloplacha.2021.103475>
- Giosan L, Donnelly JP, Vespremeanu EI, Bhattacharya JP, Olariu C, Buonaiuto FS (2005) River delta morphodynamics: examples from the Danube delta. In: Giosan L, Bhattacharya JP (Eds.) *River deltas - concepts, models, and examples*, SEPM (Society for Sedimentary Geology) Special Publication. 83:87–132. https://www.who.edu/cms/files/danube-deltas_45595.pdf
- GKRH (2009) Geological Map of the Republic of Croatia, 1:300.000, 1 Sheet. Hrvatski geološki institut/Croatian Geological Survey, Zagreb. <http://webgis.hgi-cgs.hr/gk300/default.aspx>
- Gong C, Sztanó O, Steel RJ, Xian B, Galloway WE, Bada G (2018) Critical differences in sediment delivery and partitioning between marine and lacustrine basins: a comparison of marine and lacustrine aggradational to progradational clinothem pairs. *GSA Bull* 131:766–781. <https://doi.org/10.1130/B32042.1>
- Graham GH, Jackson MD, Hampson GJ (2015) Three-dimensional modeling of clinoforms in shallow-marine reservoirs: Part 1. Concepts and application. *AAPG Bull* 99(6):1013–1047. <https://doi.org/10.1306/01191513190>
- Granjeon D (2014) 3D forward modelling of the impact of sediment transport and base level cycles on continental margins and incised valleys. *Int Assoc Sedimentol Spec Publ* 46:453–472. <https://doi.org/10.1002/9781118920435.ch16>
- Granjeon D, Joseph P (1999) Concepts and applications of a 3-D multiple lithology, diffusive model in stratigraphic modeling. *Soc Sediment Geol Spec Publ*. <https://doi.org/10.2110/pec.99.62.0197>
- Grizelj A, Peh Z, Tibljaš D, Kovačić M, Kurečić T (2016) Mineralogical and geochemical characteristics of Miocene pelitic sedimentary rocks from the south-western part of the Pannonian Basin System (Croatia): Implications for provenance studies. *GSF* 8(1):65–80. <https://doi.org/10.1016/j.gsf.2015.11.009>
- Gvirtzman Z, Csato I, Granjeon D (2014) Constraining sediment transport to deep marine basins through submarine channels: the levant margin in the Late Cenozoic. *Mar Geol* 347:12–26. <https://doi.org/10.1016/j.margeo.2013.10.010>
- Harzhauser M, Mandić O (2008) Neogene lake systems of Central and South-Eastern Europe: faunal diversity, gradients and interrelations. *Palaeogeogr Palaeoclimatol Palaeoecol* 260:417–434. <https://doi.org/10.1016/j.palaeo.2007.12.013>
- Helland-Hansen W, Hampson GJ (2009) Trajectory analysis and applications. *Basin Res* 21:454–483. <https://doi.org/10.1111/j.1365-2117.2009.00425.x>
- Henriksen S, Helland-Hansen W, Bullimore S (2011) Relationships between shelf-edge trajectories and sediment dispersal along depositional dip and strike: a different approach to sequence stratigraphy. *Basin Res* 23(1):3–21. <https://doi.org/10.1111/j.1365-2117.2010.00463.x>
- Horvat M, Klötzli U, Jamičić D, Buda G, Klötzli E, Hauzenberger C (2018) Geochronology of granitoids from Psunj and Papuk mts. *Croatia Geochronometria* 45:198–210. <https://doi.org/10.1515/geochr-2015-0099>
- Horváth F (1995) Phases of compression during the evolution of the Pannonian Basin and its bearing on hydrocarbon exploration. *Mar Pet Geol* 12(8):837–844. [https://doi.org/10.1016/0264-8172\(95\)98851-U](https://doi.org/10.1016/0264-8172(95)98851-U)
- Horváth F, Bada G, Szafián P, Tari G, Ádám A, Cloetingh S (2006) Formation and deformation of the Pannonian Basin: constraints from observational data. *Geol Soc Lond Mem* 32:191–206. <https://doi.org/10.1144/GSL.MEM.2006.032.01.11>
- Horváth F, Musitz B, Balázs A, Véghe A, Uhrin A, Nádor A, Koroknai B, Pap N, Tóth T, Wórum G (2015) Evolution of the Pannonian basin and its geothermal resources. *Geothermics* 53:328–352. <https://doi.org/10.1016/j.geothermics.2014.07.009>
- Jarosinski M, Beekman F, Matenco L, Cloetingh S (2011) Mechanics of basin inversion: finite element modelling of the Pannonian Basin System. *Tectonophysics* 502(1–2):121–145. <https://doi.org/10.1016/j.tecto.2009.09.015>
- Jones GE, Hodgson DM, Flint SS (2015) Lateral variability in clinoform trajectory, process regime, and sediment dispersal patterns beyond the shelf-edge rollover in exhumed basin margin-scale clinothems. *Basin Res* 27(6):657–680. <https://doi.org/10.1111/bre.12092>
- Joniak P, Šujan M, Fordinál K, Braucher R, Rybár S, Kováčová M, Kováč M (2020) The age and paleoenvironment of a late miocene floodplain alongside Lake Pannon: Rodent and mollusk biostratigraphy coupled with authigenic ¹⁰Be/⁹Be dating in the northern Danube Basin of Slovakia. *Palaeogeogr Palaeoclimatol Palaeoecol*. <https://doi.org/10.1016/j.palaeo.2019.109482>
- Juhász E, Müller P, Tóth-Makk Á, Hámor T, Farkas-Bulla J, Sütö-Szentai M, Phillips RL, Ricketts B (1996) High-resolution sedimentological and subsidence analysis of the Late Neogene, Pannonian Basin. *Hungary Acta Geol Hung* 39(2):129–152
- Juhász G, Pogácsás G, Magyar I, Vakarcs G (2007) Tectonic versus climatic control on the evolution of fluvio-deltaic systems in a lake basin, Eastern Pannonian Basin. *Sediment Geol* 202(1–2):72–95. <https://doi.org/10.1016/j.sedgeo.2007.05.001>
- Kamenski A, Cvetković M, Kolenković Močilac I, Saftić B (2020) Lithology prediction in the subsurface by artificial neural networks on well and 3D seismic data in clastic sediments: a stochastic approach to a deterministic method. *GEM*. <https://doi.org/10.1007/s13137-020-0145-3>
- Kovačić M, Pavelić D (2017) Neogene stratigraphy of Slavonian mountains. In: Kovačić M, Wacha L, Horvat M (eds) *Fieldtrip guidebook: Neogene of Central and South-Eastern Europe*. Croatian Geological Society, Zagreb, pp 5–9
- Kovačić M, Zupanić J, Vrsaljko D, Miknić M, Bakrač K, Hećimović I, Avanić R, Brkić M (2004) Lacustrine basin to delta evolution in the Zagorje Basin, a Pannonian sub-basin (Late Miocene: Pontian, NW Croatia). *Facies* 50:19–33
- Kovačić M, Horvat M, Pikija M, Slovenec D (2011) Composition and provenance of Neogene sedimentary rocks of Dilj gora Mt. (south Pannonian Basin Croatia). *Geol Croat*. <https://doi.org/10.4154/GC.2011.10>
- Kovács A, Balázs A, Špelić M, Sztanó O (2021) Forced or normal regression signals in a lacustrine basin? Insights from 3D stratigraphic forward modeling in the SW Pannonian Basin. *Glob Planet Change*. <https://doi.org/10.1016/j.gloplacha.2020.103376>
- Kroonenberg, SB, Simmons MD, Alekseevski, NI, Aliyeva E, Allen MB, Aybulatov DN, Baba-Zadeh A, Babyukova EN, Davies CE, Hinds DJ, Hoogendoorn RM, Huseynov D, Ibrahimov B., Mamedov P, Overeem I, Rusakov GV, Suleymanova SF, Svitoch AA, Vincent SJ (2005) Two deltas, two basins, one river, one sea: the modern Volga delta as an analogue of the Neogene productive series, South Caspian Basin. In: Giosan L, Bhattacharya JP (Eds.), *SEPM Special Publication: River Deltas—Concepts, Models and Examples*. SEPM, USA, Oklahoma, Tulsa, 231–256.

- Lučić D, Saftić B, Krizmanić K, Prelogović E, Britvić V, Mesić I, Tadej J (2001) The Neogene evolution and hydrocarbon potential of the Pannonian Basin in Croatia. *Mar Pet Geol* 18(1):133–147. [https://doi.org/10.1016/S0264-8172\(00\)00038-6](https://doi.org/10.1016/S0264-8172(00)00038-6)
- Madof AS, Harris DA, Connell DS (2016) Nearshore along-strike variability: Is the concept of the systems tract unhinged? *Geology* 44(4):315–318. <https://doi.org/10.1130/G37613.1>
- Magyar I (2021) Chronostratigraphy of clinothem-filled non-marine basins: dating the Pannonian stage. *Glob Planet Change* 205:1–10. <https://doi.org/10.1016/j.gloplacha.2021.103609>
- Magyar I, Sztano O (2008) Is there a Messinian unconformity in the Central Paratethys? *Stratigraphy* 5:247–257
- Magyar I, Geary DH, Muller P (1999) Paleogeographic evolution of the Late Miocene Lake Pannon in Central Europe. *Palaeogeogr Palaeoclimatol Palaeoecol* 151–167.
- Magyar I, Radivojević D, Sztano O, Synak R, Ujszászi K, Pócsik M (2013) Progradation of the paleo-Danube shelf margin across the Pannonian Basin during the Late Miocene and Early Pliocene. *Global Planet Change* 103:168–173. <https://doi.org/10.1016/j.gloplacha.2012.06.007>
- Magyar I, Krezsek C, Tari G (2019) Clinoforms as paleogeographic tools: development of the Danube catchment above the deep Paratethyan basin in Central and Southeast Europe. *Basin Res* 32:320–331. <https://doi.org/10.1111/bre.12401>
- Malvić T, Cvetković M (2013) Lithostratigraphic units in the Drava depression (Croatian and Hungarian parts)—a correlation. *Nafta* 64(1):27–33
- Mandić O, Kurečić T, Neubauer TA, Harzhauser M (2015) Stratigraphic and palaeogeographic significance of lacustrine molluscs from the Pliocene *Viviparus* beds in central Croatia. *Geol Croat* 68(3):179–207. <https://doi.org/10.4154/GC.2015.15>
- Mandić O, Lj R, Čorić S, Pezelj Đ, Theobald D, Sant K, Krijgsman W (2019) AGE and mode of the middle miocene marine flooding of the Pannonian Basin—constraints from Central Serbia. *Palaios* 34(2):71–95. <https://doi.org/10.2110/palo.2018.052>
- Márton E, Pavelić D, Tomljenović B, Avanić R, Pamić J, Márton P (2002) In the wake of a counterclockwise rotating Adriatic microplate: Neogene paleomagnetic results from northern Croatia. *Int J Earth Sci* 91:514–523. <https://doi.org/10.1007/s00531-001-0249-4>
- Matoš B, Pérez-Peña JV, Tomljenović B (2016) Landscape response to recent tectonic deformation in the SW Pannonian Basin: evidence from DEM-based morphometric analysis of the Bilogora Mt. area, NE Croatia. *Geomorphology* 263:132–155. <https://doi.org/10.1016/j.geomorph.2016.03.020>
- Mattick RE, Rumpler J, Phillips RL (1985) Seismic stratigraphy of the Pannonian Basin in southeastern Hungary. *Geophys Trans* 31:13–54
- Nyíri D, Tókéš L, Zdravcevcz C, Fodor L (2021) Early post-rift confined turbidite systems in a supra-detachment basin: Implications for the early to middle Miocene basin evolution and hydrocarbon exploration of the Pannonian Basin. *Glob Planet Change*. <https://doi.org/10.1016/j.gloplacha.2021.103500>
- Overeem I, Kroonenberg SB, Veldkamp A, Groenesteijn K, Ruskov GV, Svitoch AA (2003) Small-scale stratigraphy in a large ramp delta: recent and Holocene sedimentation in the Volga Delta, Caspian Sea. *Sediment Geol* 159(3–4):133–157. [https://doi.org/10.1016/S0037-0738\(02\)00256-7](https://doi.org/10.1016/S0037-0738(02)00256-7)
- Pamić J, Mckee HE, Bullen DT, Lanphere AM (1995) Tertiary volcanic rocks from the Southern Pannonian Basin. *Croatia Int Geol Rev* 37(3):259–283. <https://doi.org/10.1080/00206819509465404>
- Patruno S, Helland-Hansen W (2018) Clinoforms and clinoform systems: review and dynamic classification scheme for shorelines, subaqueous deltas, shelf edges and continental margins. *Earth-Sci Rev*. <https://doi.org/10.1016/j.earscirev.2018.05.016>
- Paumard V, Bourget J, Payenberg T, George DA, Ainsworth RB, Lang S (2019) From quantitative 3D seismic stratigraphy to sequence stratigraphy: Insights into the vertical and lateral variability of shelf-margin depositional systems at different stratigraphic orders. *Mar Pet Geol* 110:797–831. <https://doi.org/10.1016/j.marpetgeo.2019.07.007>
- Paumard V, Bourget J, Payenberg T, George DA, Ainsworth RB, Lang S, Posamentier HW (2020) Controls on deep-water sand delivery beyond the shelf-edge: accommodation, sediment supply, and deltaic progress regime. *J Sediment Res* 90:104–130. <https://doi.org/10.2110/jsr.2020.2>
- Pavelić D (2001) Tectonostratigraphic model for the North Croatian and North Bosnian sector of the Miocene Pannonian basin system. *Basin Res* 12:359–376. <https://doi.org/10.1046/j.0950-091x.2001.00155.x>
- Pavelić D, Kovačić M (2018) Sedimentology and stratigraphy of the Neogene rift-type North Croatian Basin (Pannonian Basin System, Croatia): a review. *Mar Pet Geol* 91:455–469. <https://doi.org/10.1016/j.marpetgeo.2018.01.026>
- Pellegrini C, Asioli A, Bohacs KM, Drexler TM, Feldman HR, Sweet ML, Maselli V, Rovere M, Gamberi F, Dalla Valle G, Trincardi F (2018) The late Pleistocene Po River lowstand wedge in the Adriatic Sea: controls on architecture variability and sediment partitioning. *Mar Pet Geol* 96:16–50. <https://doi.org/10.1016/j.marpetgeo.2018.03.002>
- Porebski SJ, Steel RJ (2003) Shelf-margin deltas: their stratigraphic significance and relation to deepwater sands. *Earth Sci Rev* 62(3–4):283–326. [https://doi.org/10.1016/S0012-8252\(02\)00161-7](https://doi.org/10.1016/S0012-8252(02)00161-7)
- Posamentier HW, Allen GP (1993) Variability of the sequence stratigraphic model: effects of local basin factors. *Sediment Geol* 1–2:91–109. [https://doi.org/10.1016/0037-0738\(93\)90135-R](https://doi.org/10.1016/0037-0738(93)90135-R)
- Posamentier HW, Allen GP (1999) *Siliciclastic sequence stratigraphy: concepts and applications*, vol 7. SEPM, Oklahoma, Tulsa, USA. <https://doi.org/10.2110/csp.99.07>
- Prelogović E, Saftić B, Kuk V, Velić J, Dragaš M, Lučić D (1998) Tectonic activity in the Croatian part of the Pannonian basin. *Tectonophysics* 297(1–4):283–293. [https://doi.org/10.1016/S0040-1951\(98\)00173-5](https://doi.org/10.1016/S0040-1951(98)00173-5)
- Radivojević D, Radonjić M, Katona LT, Magyar I (2022) Against the tide: southeast to northwest shelf-edge progradation in the southeastern margin of Lake Pannon, Banat (Serbia and Romania). *Int J Earth Sci* 111:1551–1671. <https://doi.org/10.1007/s00531-022-02188-z>
- Rich JL (1951) Three critical environments of deposition and criteria for recognition of rocks deposited in each of them. *Geological Soc Am Bull* 62:1–20
- Rögl F, Steininger FF (1983) Vom Zerfall der Tethys zu Mediterran und Paratethys. *Die Neogene Palaeogeographie und Palinspastik des zirkum-mediterranen Raumes*. *Ann Naturhist Mus Wien* 85:135–163
- Sacchi M, Horváth F, Magyari O (1999) Role of unconformity-bounded units in the stratigraphy of the continental record: a case study from the Late Miocene of the western Pannonian Basin, Hungary. *Geol Soc Spec Publ*. <https://doi.org/10.1144/GSL.SP.1999.156.01.17>
- Saftić B, Velić J, Sztano O, Juhász G, Ivković Ž (2003) Tertiary subsurface facies, source rocks and hydrocarbon reservoirs in the SW Part of the Pannonian Basin (Northern Croatia and South-Western Hungary). *Geol Croat* 56(1):101–122. <https://doi.org/10.4154/232>
- Sant K, Palcu DV, Mandić O, Krijgsman W (2017) Changing seas in the early-middle Miocene of Central Europe: a mediterranean

- approach to paratethyan stratigraphy. *Terra Nova* 29(5):273–281. <https://doi.org/10.1111/ter.12273>
- Sebe K (2021) Structural features in the Miocene sediments of the Pécs–Danitzpuszta sand pit (SW Hungary). *Földtani Közleány*. <https://doi.org/10.23928/foldt.kozl.2021.151.4.411>
- Sebe K, Kovačić M, Magyar I, Krizmanić K, Špelić M, Bigunac D, Sütő-Szentai M, Kovács A, Szuromi-Korecz A, Bakrač K, Hajek-Tadesse V, Troskot-Čorbić T, Sztanó O (2020) Correlation of upper Miocene-Pliocene Lake Pannon deposits across the Drava Basin, Croatia and Hungary. *Geol Croat* 73(3):177–195. <https://doi.org/10.4154/gc.2020.12>
- Šimon J (1973) O nekim rezultatima regionalne korelacije litostratigrafskih jedinica u jugozapadnom području Panonskog bazena. *Nafta* 12:623–630
- Šujan M, Braucher R, Tibenský M, Fordinál K, Rybár S, Kováč M, Aster Team (2020) Effects of spatially variable accommodation rate on channel belt distribution in an alluvial sequence: authigenic $^{10}\text{Be}/^{9}\text{Be}$ -based Bayesian age-depth models applied to the upper Miocene Volkovce Fm. (northern Pannonian Basin System, Slovakia). *Sediment Geol*. <https://doi.org/10.1016/j.sedgeo.2019.105566>
- Sztanó O, Magyar I (2007) Deltaic parasequences on gamma logs, ultra-high resolution seismic images and outcrops of lake pannon deposits. *Joannea Geol Palaont* 9:105–108
- Sztanó O, Szafián P, Magyar I, Horányi A, Bada G, Hughes WH, Hoyer LD, Wallis JR (2013a) Aggradation and progradation controlled clinothems and deep-water sand delivery model in the Neogene lake pannon Makó Trough, Pannonian Basin SE, Hungary. *Glob Planet Change* 103:149–167. <https://doi.org/10.1016/j.gloplacha.2012.05.026>
- Sztanó O, Magyar I, Szónoky M, Lantos M, Müller P, Lenkey L, Katona L, Csillag G (2013b) Tihany Formation in the surroundings of Lake Balaton: type locality, depositional setting and stratigraphy. *Földtani Közleány* 143(1):73–98
- Sztanó O, Sebe K, Csillag G, Magyar I (2015) Turbidites as indicators of paleotopography, upper Miocene Lake Pannon, Western Mecsek Mountains (Hungary). *Geol Carpath* 66:331–344. <https://doi.org/10.1515/geoca-2015-0029>
- Sztanó O, Kováč M, Magyar I, Šujan M, Fodor L, Uhrin A, Rybár S, Csillag G, Tőkés L (2016) Late Miocene sedimentary record of the Danube/Kisalföld Basin: interregional correlation of depositional systems, stratigraphy and structural evolution. *Geol Carpath* 67(6):525–542. <https://doi.org/10.1515/geoca-2016-0033>
- Sztanó O, Magyar I, Katona L (2020) A Pannon-tó és a Balaton. In: Babinszki E, Horváth F (eds.) *A Balaton kutatása Lóczy Lajos nyomdokán*. Magyarhoni Földtani Társulat, 107–126.
- Tari V, Pamić J (1998) Geodynamic evolution of the northern Dinarides and the southern part of the Pannonian Basin. *Tectonophysics* 297(1–4):269–281. [https://doi.org/10.1016/S0040-1951\(98\)00172-3](https://doi.org/10.1016/S0040-1951(98)00172-3)
- ter Borgh M, Vasiliev I, Stoica M, Knežević S, Maţenco L, Krijgsman W, Rundić L, Cloetingh S (2013) The isolation of the Pannonian basin (Central Paratethys): new constraints from magnetostratigraphy and biostratigraphy. *Glob Planet Change* 103:99–118. <https://doi.org/10.1016/j.gloplacha.2012.10.001>
- ter Borgh M, Radivojević D, Matenco L (2014) Constraining forcing factors and relative sea-level fluctuations in semi-enclosed basins: the Late Neogene demise of Lake Pannon. *Basin Res* 27(6):681–695. <https://doi.org/10.1111/bre.12094>
- Tesch P, Reece SR, Markello RJ, Carlos Laya J, Pope CM (2019) Adding the missing third and fourth dimensions to trajectory analysis in carbonate systems. *Basin Res* 32:388–401. <https://publons.com/publon/>. <https://doi.org/10.1111/bre.12422>
- Tomljenović B, Csontos L (2001) Neogene-quaternary structures in the border zone between Alps, Dinarides and Pannonian Basin (Hrvatsko zagorje and Karlovac basins, Croatia). *Int J Earth Sci* 90:560–578. <https://doi.org/10.1007/s005310000176>
- Törő B, Sztanó O, Fodor I, (2012) Inherited and syndepositional structural control on the evolution of the slope of Lake Pannon, Northern Somogy, Hungary. *Földtani Kozlony* 142:339–356
- Uhrin A, Sztanó O (2012) Water-level changes and their effect on deep-water sand accumulation in a lacustrine system: a case study from the Late Miocene of western Pannonian Basin, Hungary *Int J Earth Sci* 101:1427–1440. <https://doi.org/10.1007/s00531-011-0741-4>
- Uhrin A, Magyar I, Sztanó, (2009) Control of the Late Neogene (Pannonian s.l.) sedimentation by basement deformation in the Zala Basin. *Földtani Közleány* 193(3):273–282
- Utescher T, Erdei B, Hably L, Mosbrugger V (2017) Late Miocene vegetation of the Pannonian Basin. *Palaeogeogr Palaeoclimatol Palaeoecol* 467:131–148. <https://doi.org/10.1016/j.palaeo.2016.02.042>
- Vági D, Csicsák P, Varga G, Magyar I, Sztanó O (2019) Angle and architecture of merging slopes: implications on deep-water sediment accumulations. American Association of Petroleum Geologists, Europe Regional Conference, Paratethys petroleum systems between Central Europe and the Caspian region, Book of Abstracts Austria, Vienna, 134.
- Vail PR, Mitchum Jr RM, Thompson III S (1977) Seismic stratigraphy and global changes of sea level, Part 4: global cycles of relative changes of sea level. In: Payton, C.E. (Ed.), *Seismic Stratigraphy—Applications to Hydrocarbon Exploration*, AAPG Memoir 26:83–97
- Vakarc G, Vail PR, Tari G, Gy P, Mattick RE, Szaboá A (1994) Third-order Middle Miocene-Early Pliocene depositional sequences in the prograding delta complex of the Pannonian Basin. *Tectonophysics* 240:81–106. [https://doi.org/10.1016/0040-1951\(94\)90265-8](https://doi.org/10.1016/0040-1951(94)90265-8)
- Vasiliev I, Bakrač K, Kovačić M, Abdul Aziz H, Krijgsman W (2007) Paleomagnetic results from the Sarmatian/Pannonian boundary in the North-Eastern Croatia (Vranović Section, Našice Quarry). *Geol Croat* 60(2):151–163. <https://doi.org/10.4154/GC.2007.04>
- Velić J, Malvić T, Cvetković M, Vrbanc B (2012) Reservoir geology, hydrocarbon reserves and production in the Croatian part of the Pannonian Basin System. *Geol Croat* 65(1):91–101. <https://doi.org/10.4154/GC.2012.07>
- Vrbanc B, Velić J, Malvić T (2010) Sedimentation of deep-water turbidites in the SW part of the Pannonian Basin. *Geol Carpath* 61(1):55–69. <https://doi.org/10.2478/v10096-010-0001-8>
- Zecchin M, Catuneanu O (2020) High-resolution sequence stratigraphy of clastic shelves VII: 3D variability of stacking patterns. *Mar Pet Geol*. <https://doi.org/10.1016/j.marpetgeo.2020.104582>